Electronic Supplementary Material (ESI) for New Journal of Chemistry.

Electronic Supplementary

Amide probe as selective Al^{3+} and Fe^{3+} sensor inside the HeLa, and a549 cell lines: Pictet-Spengler reaction for rapid detection of tryptophan amino acid

Bidyut Kumar Kundu,[a] Rinky Singh,[a] Ritudhwaj Tiwari,[b] Debasis Nayak,[b] Suman Mukhopadhyay[a, b,*]

[a] *Department of Chemistry, School of Basic Sciences, Indian Institute of Technology Indore, Khandwa Road, Simrol, Indore 452020, India. Tel: +91 731 2438 735 Fax: +91 731 2361 482 E-mail: suman@iiti.ac.in*

[b] *Centre for Biosciences and Biomedical Engineering, School of Basic Sciences, Indian Institute of Technology Indore, Khandwa Road, Simrol, Indore 452020, India.*

Table of contents

Abbreviation used in this article:

Entry	*Significance*	*Entry*	*Significance*
L	N-4-pyridinyl-1-isoquinolinecarboxamide	**PL/ FL**	Photo luminance/ Fluorescence
PET	Photo induced electron transfer	**Aq.**	Aqueous
DFT/ TD-DFT	Density functional theory/ Time dependent-density functional theory	**HeLa**	Human cervical cancer cell lines
NMR	Nuclear magnetic resonance	**XRD**	X-ray diffraction
ESI-MS	Electrospray ionisation mass spectrometry	**UV-Vis**	Ultraviolet-Visible
FTIR	Fourier transformed infra-red	**Conc.**	Concentration
[L]/ [M^{3+}]	Concentration of probe or metal(s)	**a549**	lung cancer cell lines
ICT	Intramolecular charge transfer	**h/ hrs.**	Hour/ Hours
LOD	Limit of detection/ detection limit	**r.t.**	Room temperature
CHEF	Chelation-enhanced fluorescence	**equiv.**	Equivalents
MLCT	Metal to ligand charge transfer	**eqn.**	Equation
WHO	World health organisation	**CD**	Circular Dichroism
PET	Photo induced electron/energy transfer	**ns/ min**	Nano seconds/ minutes
ICP	Inductively coupled plasma	**[M^{n+}]**	Metal ion concentration
TGA	Thermogravimetric Analysis	**e^-**	Electron
LUMO	Lowest unoccupied molecular orbital	**HOMO**	Highest occupied molecular orbital
λ_{ex} or λ_{em}	Excitation or emission wavelength maxima	**CV**	Cyclic voltammetry

Experimental Section:

Materials

All reagents and solvents were purchased from commercial sources and used as received unless stated otherwise. Mili-Q water was used throughout the experiment. The solutions of the metal ions were prepared from their nitrate salts, except for Cr^{3+} and Ru^{3+}, which were used as chloride salts.

Apparatus and Procedures

The measurements of pH have been done using a digital pH meter (TOSHCON INDUSTRIES PVT. LTD., AJMER). Absorption spectra were performed on a Varian UV-Vis spectrophotometer (Model: Cary 100). Fluorescence emission spectra were recorded at 25.0 ± 0.2 ºC on a Fluoromax-4p spectrofluorometer from Horiba JobinYvon (Model: FM-100) using a quartz cuvette with a path length of 2 cm. ^{1}H and ^{13}C NMR spectra were recorded on an AVANCE III 400 Ascend Bruker BioSpin machine at ambient temperature with tetramethylsilane (TMS, 0.00 ppm) as an internal standard. Infrared spectra (4000 to 500 cm^{-1}) were recorded with a BRUKER TENSOR 27 instrument in KBr pellets. Field emission scanning electron microscopic study was performed on Carl Zeiss Microscope (model-Supra 55). Circular dichroism spectral analysis were recorded with JASCO J815 instrument at 298K. Crystalline nature and PXRD patterns of prepared heterogeneous catalysts were recorded on PAN analytical X"Pert Dual Goniometer diffractometer by using X'celerator solid state detector for the experiments with monochromatic Cu-Kα radiation (λ = 1.542Å) and a Ni filter. Thermogravimetric analysis (TGA) were accompanied on a "METTLER TOLEDO" TGA/DSC 1 Module with a heating rate of 10 °C min^{-1} with a sensitivity of 10 mg in the temperature range of 0-800 °C and the TGA data was analysed by "STAR^{e} Software" under a static N_2 atmosphere. Voltammetric experiments were completed using a CHI 104 electrochemical workstation (CH Instruments Model CHI62OD series). The fluorescence images of cells were taken using an Olympus Confocal laser scanning microscopy with an objective lens (×40).

- **Sample preparation for UV-vis and fluorescence titrations**

To record UV-vis as well as fluorescence spectra, 1.0 mM solution (stock solution) was prepared by dissolving 0.01 mmol of receptor L (2.49 mg) in 10 mL mixed solvent of Water-MeOH (9/1, v/v). 30 μL of stock solution was taken and diluted up to 3 mL to get 10 μM solution. On the other

hand, 0.1 mmol of $Al(NO_3)_3.9H_2O$ (37.5 mg) or $Fe(NO_3)_3.9H_2O$ (40.4 mg) was dissolved in deionized H_2O (10 mL) to obtain a 10 mM solution. 2.0-60 µL of the Al^{3+} or Fe^{3+} ion solutions (10 mM) were added to a fixed volume (30 µL) of 10 µM solution of probe L. UV-vis spectra were taken at r.t after mixing them (either probe and metal ions or amino acids) for constant time interval.

- **Competition with other metal ions and amino acids**

To find out the fluorescence active metal ions, various metal salts of a fixed concentration (0.01 mmol conc. of probe L (2.49 mg in 10 mL) solution was prepared in water : MeOH (10 mL; 9/1, v/v) and 30 µL of it (1 mM) was diluted with 2.97 mL HEPES buffer solution (10 mM) resulting the conc. of 10 µM.) were added to L to undergo corresponding UV-Vis and FL spectroscopic analysis. The stock solution of different metal salts *viz.* Li^+, Na^+, K^+, Ag^+, Mg^{2+}, Ba^{2+}, Ca^{2+}, Cu^{2+}, Ni^{2+}, Zn^{2+}, Mn^{2+}, Cd^{2+}, Hg^{2+}, Pb^{2+}, Pd^{2+}, Pt^{2+}, Al^{3+}, Ce^{3+}, Co^{3+}, Cr^{3+}, Dy^{3+}, Fe^{3+}, Gd^{3+}, La^{3+}, Pr^{3+}, Sm^{3+} and Ru^{3+} were prepared in deionized H_2O. Then, 30 µL of each metal solution having conc. 0.1 mM was taken to the 10 µM solution of L to get 10 equiv. conc. (i.e.; 100 µM) of $[M^{n+}]$. Room temperature UV-Vis and FL spectra were recorded after constant shaking within same time interval throughout the experiments.

Amino acids (0.1 mmol) was dissolved in 10 mL of distilled water and 30 µL of the amino acid solution (10 mM) were transferred to the solution of L (10 mM) prepared above (in 3 mL). After mixing them for a few seconds, UV-Vis and PL spectra were obtained at room temperature.

- **Jobs plot measurements**

0.01 mmol of chemosensor L (2.49 mg) was dissolved in 10 mL of MeOH : H_2O (1/9, v/v) mixture. Then, a series of the receptor solution of volume 0, 10, 20, 30, 40, 50, 60, 70, 80, 90 and 100 µL were taken in different vessels. Now, Al^{3+} ion solution of 100, 90, 80, 70, 60, 50, 40, 30, 20, 10 and 0 µL quantity have been added respectively and diluted further with methanol to make the final volume of 3 mL. After shaking for a few seconds, the cuvettes were placed to record UV-Vis spectra at room temperature. Similar procedure was followed for Fe^{3+} using the solvent mixture MeOH : Water (10 mL; 1/9, v/v).

- **Binding constants using Benesi-Hildebrand plot**

Benesi-Hildebrand (B-H) plot[1] was used to evaluate the binding constants due to the formation of corresponding metal complexes using the following eqn. (i):

$1/ (F - F_0) = 1/ \{K (F_{max} - F_0) C\} + 1/ (F_{max} - F_0)$ … … (i)

Where, F_0 is the PL intensity of receptor L at the emission maximum (λ_{em} = 430 nm for Al^{3+} and 433 nm for Fe^{3+}), F is the value of various concentration dependent λ_{em}, the maximum emission intensity was denoted by F_{max}, the slope of the linear plot gives the value of K i.e. the binding constant (M^{-1}), and C denotes the conc. of the Al^{3+} or Fe^{3+} ions taken throughout the series of titration. The Benesi-Hildebrand plot of $(F_{max} - F_0)/ (F - F_0)$ vs. $1/[Al^{3+}]$ gives the value of binding constant.

- **Limit of Detection for Al^{3+} and Fe^{3+}**

Eqn. (ii) was used to calculate the LOD value based on the fluorescence emission for both the metal ions.[2]

Detection limit (DL) = $3.3\sigma/ S$ … … (ii)

Where, σ stands for the standard deviation (S_d), and S denoted the slope. Slope is obtained from the linear fit plot of PL intensity changes versus concentration of Al^{3+} or Fe^{3+} added. The UV-Vis or fluorescence emission intensity of L was recorded by several consecutive scans of the blank samples by varying conc.

- **Fluorescence Quantum Yield**

Quinine sulfate dye (Φ_R = 0.09) was used as reference to estimate the quantum yield (QY)[3, 4] values of receptor L, $L+Al^{3+}$ and $L+Fe^{3+}$ in methanol by using the eqn. (v):

$$\Phi_s = \frac{Abs_R}{Abs_S} \times \frac{Area_S}{Area_R} \times \frac{\eta_S}{\eta_R} \times \Phi_R \quad \ldots \quad \ldots \text{(v)}$$

Where 'Φ' denotes the fluorescence QY, 'Area' terms denote the integration of the fluorescence curve, 'Abs' denotes optical density and the refractive index as η (η = 1.3284 for MeOH solvent medium). Subscripts 'R' and 'S' stand for the respective parameters belonging to the experimental reference as well as the sample.

- **Density Functional Theory (DFT)**

For better understanding about the molecular orbital as well as the stoichiometric coefficient for the formation of metal complexes, all geometries and energies were calculated by using the Gaussain-09 programs. Restriction free Gas phase geometries for compounds and the sensing

mechanism were fully optimized under symmetrical conditions. The singlet ground states (S_0) of HL and complexes were optimized by DFT methods by mixing the Hartree-Fock-type theory with Becke's three parameterized Lee-Yang-Parr (B3LYP) exchange functional with the 631G+(d, p) basis set.[5, 6] Further, complexes of Al^{3+} and Fe^{3+} were treated with the basis set LANL2DZ to calculate the effective core potential associated with valence double ζ basis set of Hay and Wadt. Finally, TD-DFT method correlated the theoretical and experimental observation for the electronic spectra of the receptor and its complexes.[7]

- **Cell viability**

HeLa cell lines was collected from National Center for Cell Science (NCCS), Pune. DMEM (Lonza, Cat. No. BE12-604F) medium were used for cell culture purposes, which was supplemented by 10 % (w/v) fetal bovine serum (Sigma, Cat. No. F2442), and streptomycin/ penicillin (1% at 37 °C) and 5% CO_2 followed by the seeding of HeLa cells into 96 well tissue culture plates. Cell viability study was performed for 5 different concentrations of probe (10, 50, 100, 150, 200 μg/mL) in 24 h according to our previous report.[8] In addition, the percentage viability was calculated as per following eqn. (vi):

$$\text{Cell viability/ Cell redox activity (\%)} = \frac{O.D_{(S)} - O.D_{(B)}}{O.D_{(C)} - O.D_{(B)}} \times 100 \quad \ldots \quad \ldots \text{ (vi)}$$

Where, $O.D_{(S)}$, $O.D_{(B)}$, and $O.D_{(C)}$ are the optical density/ absorbance values of sample, blank, and control, respectively.

- **Cell imaging**

HeLa cells were harvested at the exponential growth phase and were plated into 6 well flat bottom culture plate. The cells were incubated for an additional 24 h at 37 ºC for growth and adherence of the cells. After this incubation period, the medium was then aspirated and was replaced with 2 mL of fresh optimem medium containing Al^{3+} ion (0-100 μM) and incubated for 2 h. Receptor solution (<1% DMSO solution; 20 μM) was then added and incubated for additional ½ h. DAPI solution (100 ng/mL) was introduced for the control experiment under similar environment. The cells were washed twice with PBS (pH 7.4). Images were acquired on the confocal microscope (Olympus IX 83) and analyzed using the FluoView software.[9, 10]

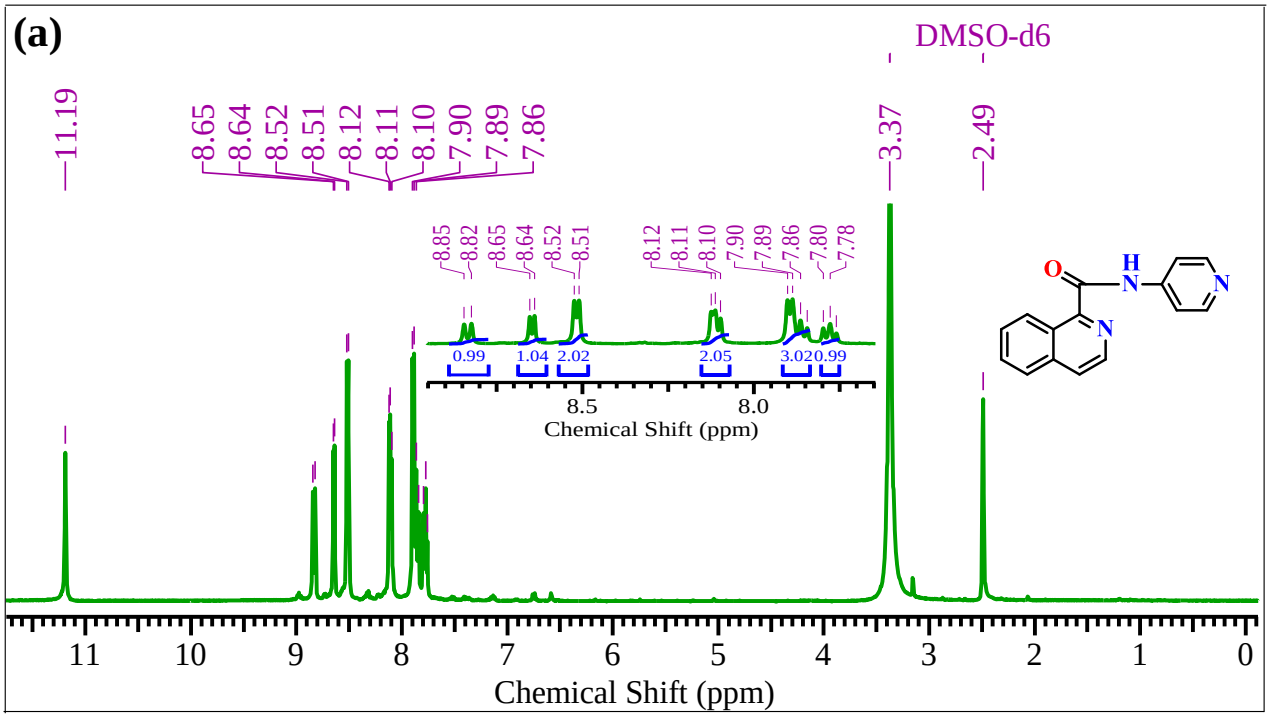
(a)
DMSO-d6
11.19
8.65
8.64
8.52
8.51
8.12
8.11
8.10
7.90
7.89
7.86
3.37
2.49
0.99
1.04
2.02
2.05
3.02
0.99
Chemical Shift (ppm)

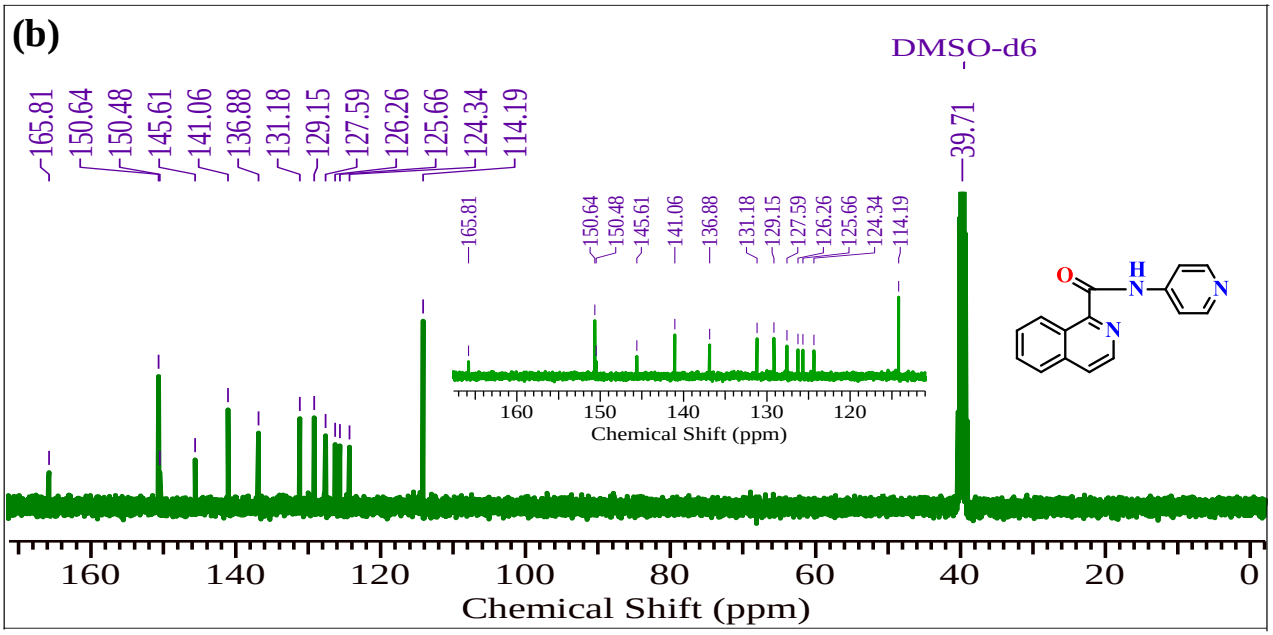
(b)
DMSO-d6
165.81
150.64
150.48
145.61
141.06
136.88
131.18
129.15
127.59
126.26
125.66
124.34
114.19
39.71
Chemical Shift (ppm)

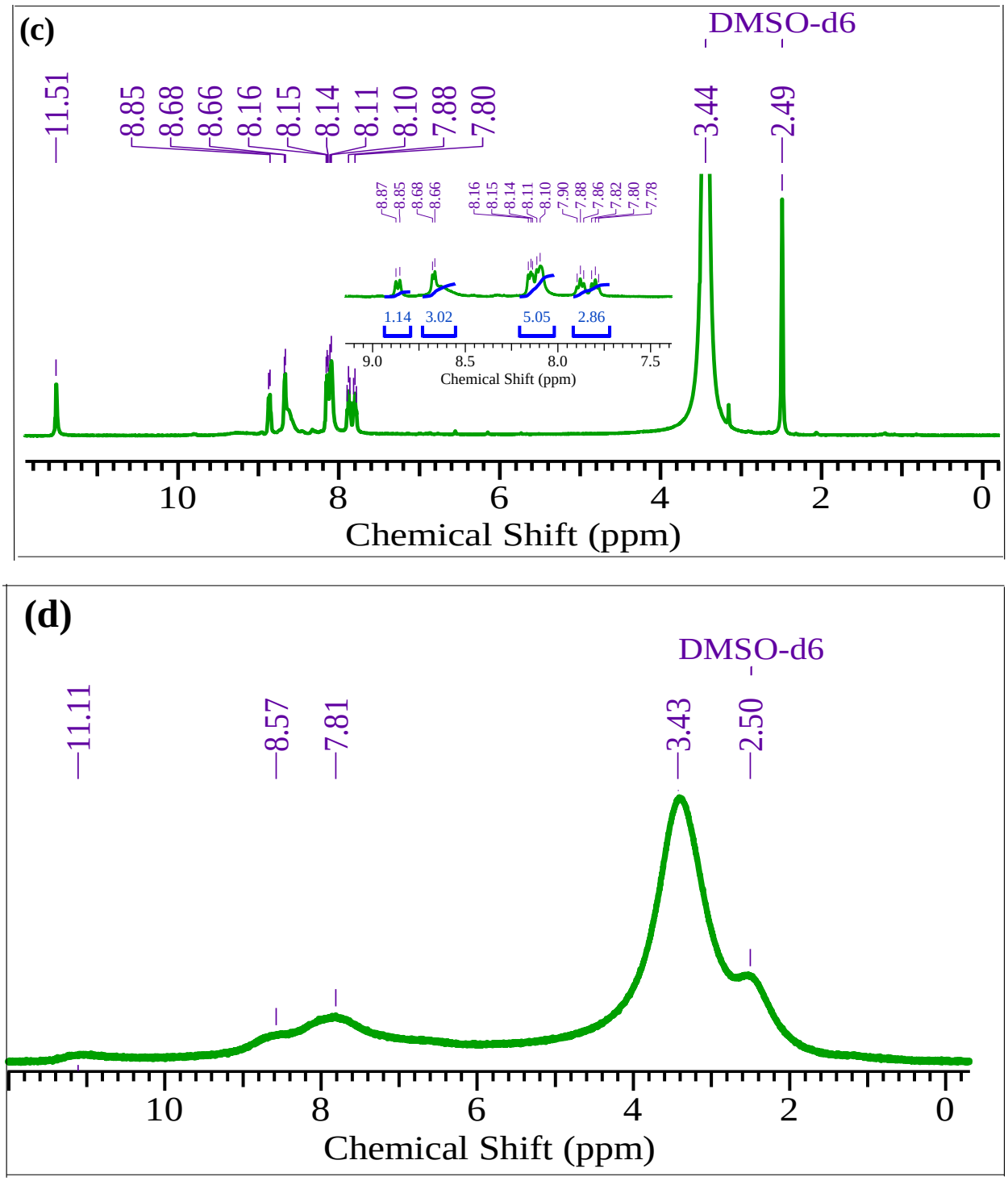

Fig. S1 NMR Spectra in DMSO-d6 at 400.13 MHz, 298K: (a) ^{1}H NMR Spectra of L and (b) ^{13}C NMR Spectra of L (c) ^{1}H NMR Spectra of Al-complex and (d) ^{1}H NMR Spectra of Fe-complex.

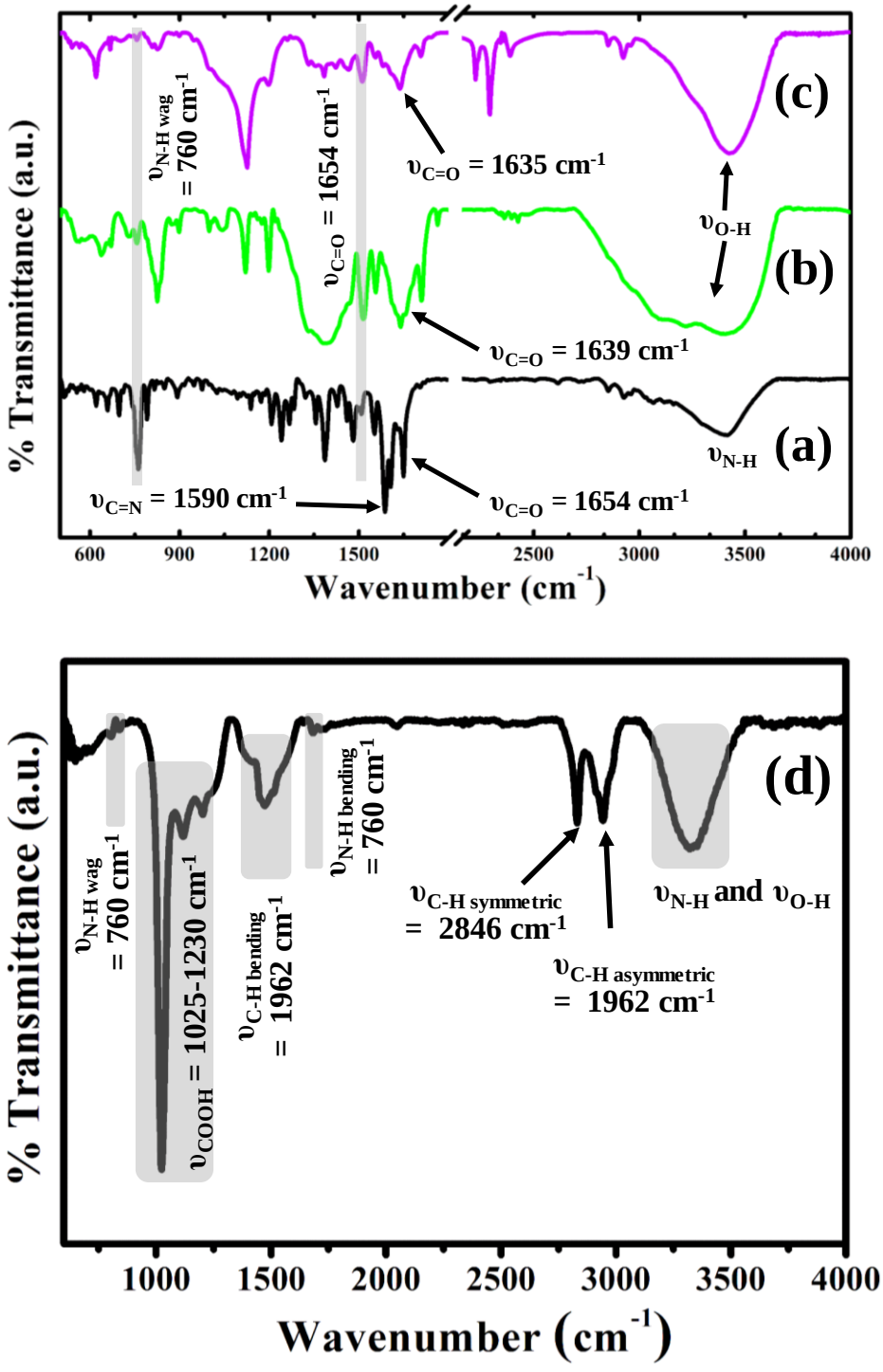

Fig. S2 FT-IR spectra of (a) probe L, (b) complex **1**, (c) complex **2** showing the amide C=O (s) and N-H (m) stretching at 1690- 1630 and 3700 cm^{-1}, and (d) PSC compound (where, 's', 'b', and 'm' signifies the strong, broad, and medium strength of frequencies).[11]

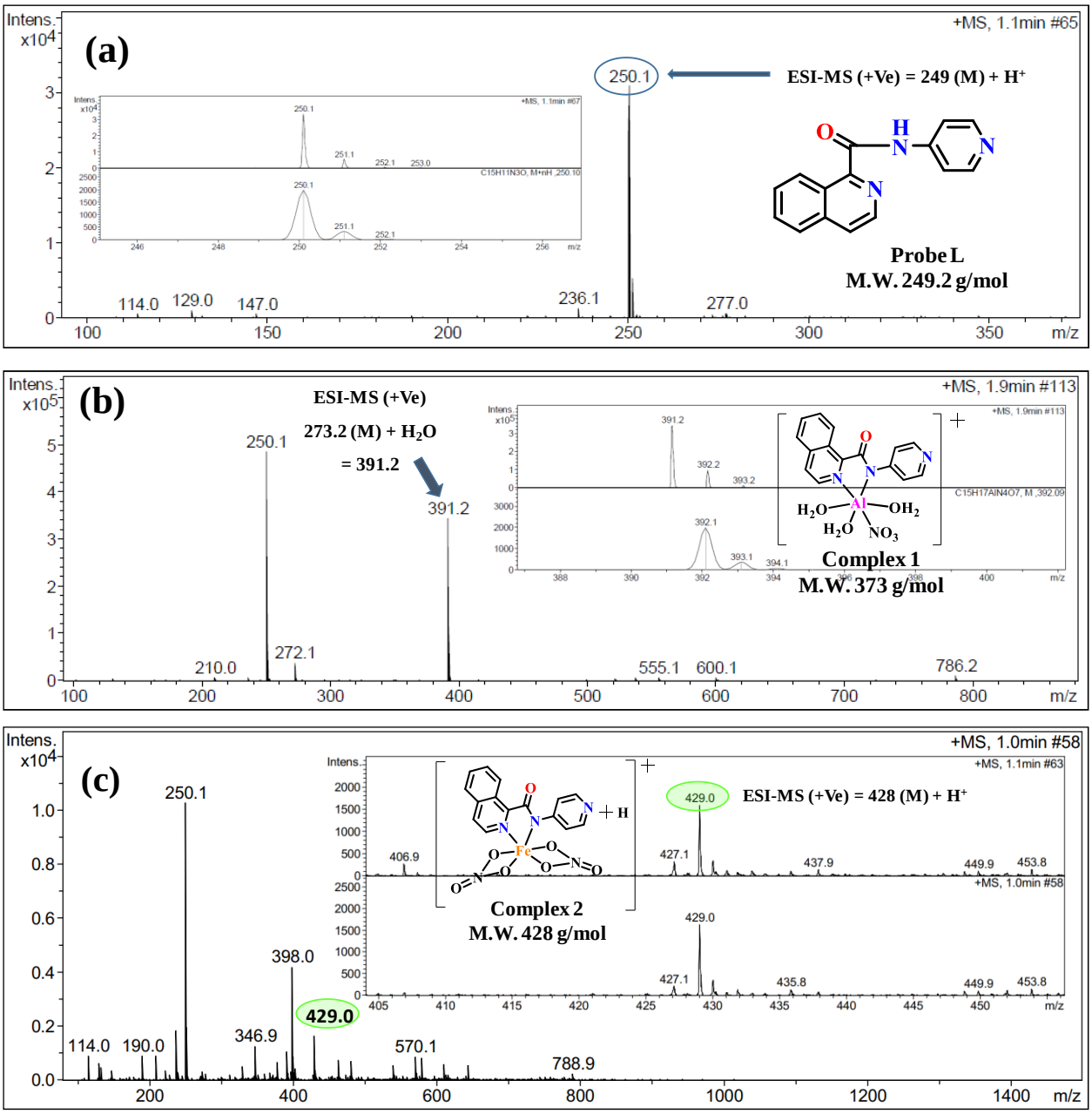

Fig. S3 ESI-MS data in positive mode (MeOH solvent) for (a) probe **L**, (b) complex **1** and (c) complex **2**.

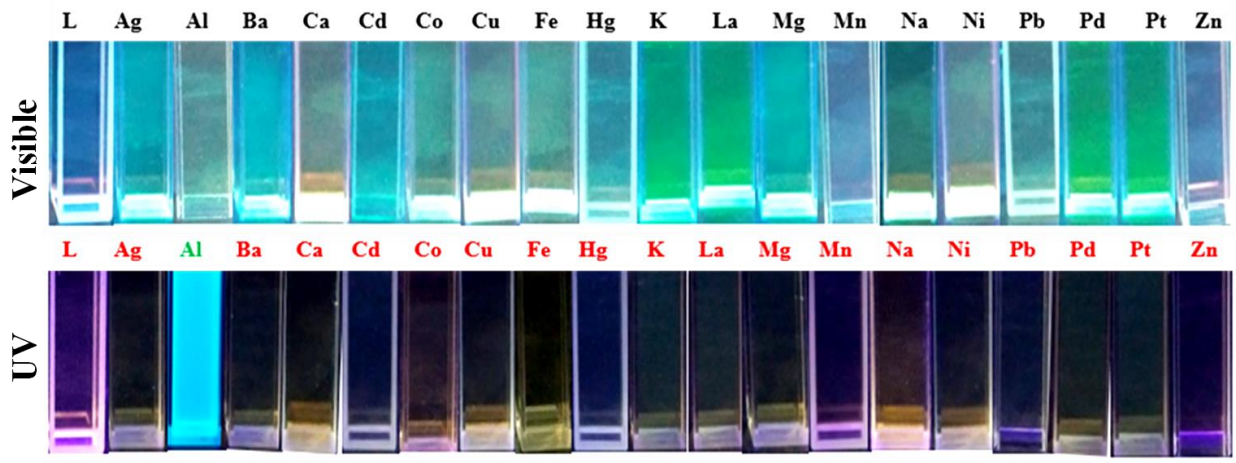

Fig. S4 Colorimetric detection under visible and UV chamber before and after addition of various metals to the probe **L**.

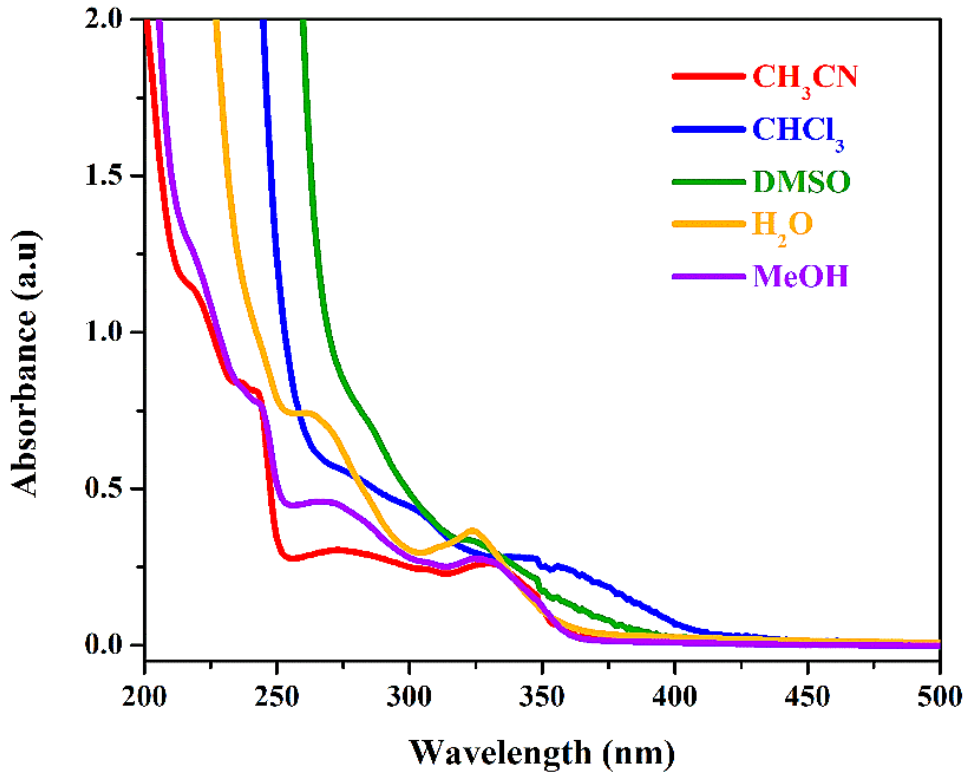

Fig. S5 Solvent dependent absorption response of amide receptor **L** (10 μM).

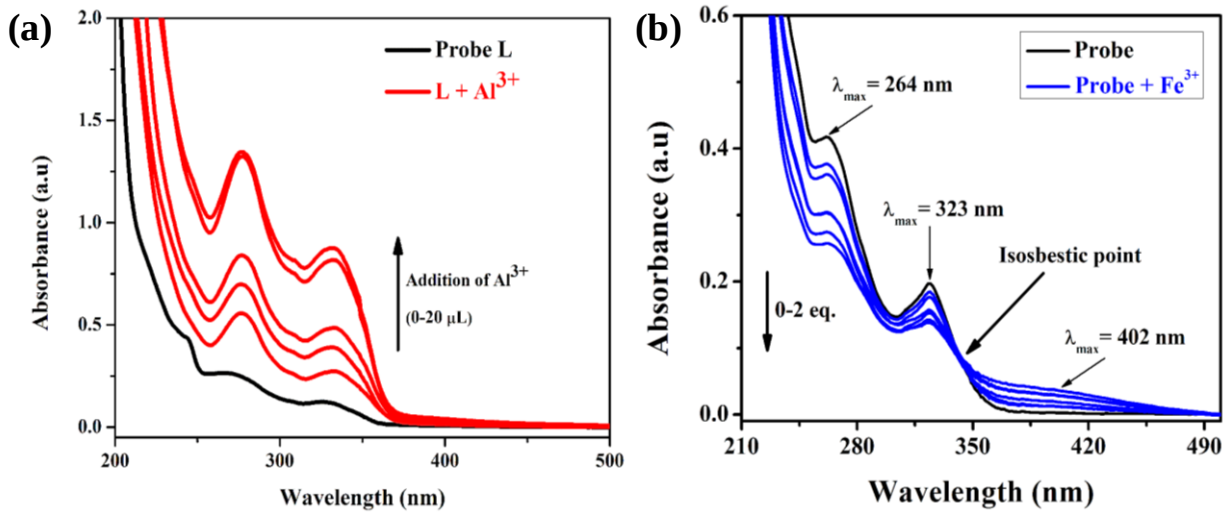

Fig. S6 Absorbance response of **L** (10 µM) upon addition of (a) Al^{3+} and (b) Fe^{3+} (0 to 15 equiv.) in MeOH : H_2O (1/9, (v/v), pH = 7.4) showing an isosbestic points for Fe^{3+} complex.

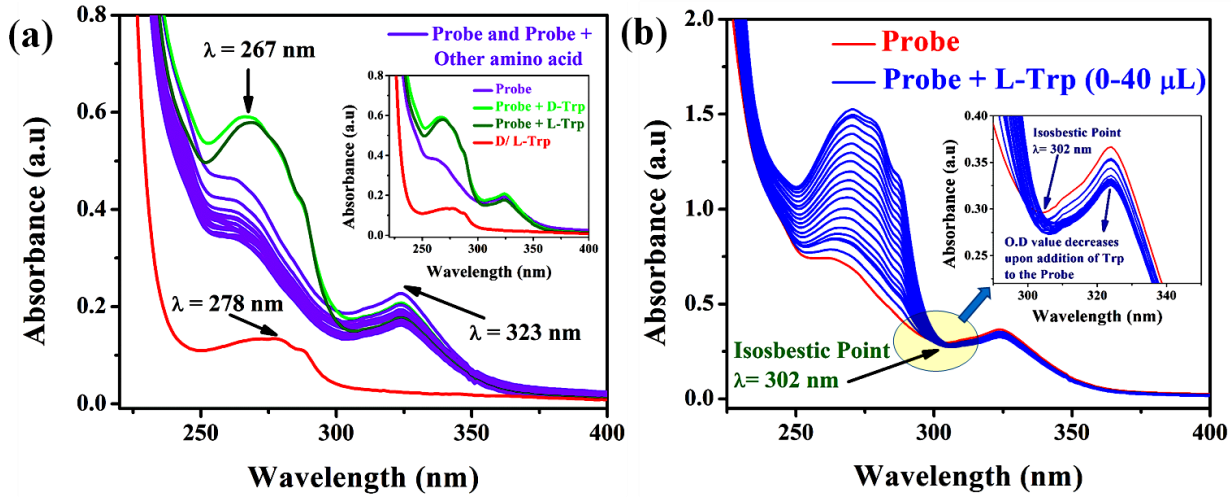

Fig. S7 (a) Electronic spectra of receptor **L** (10 µM) in CH_3OH/ HEPES buffer (at pH ~7.4; 1 : 9 (v/v)) on adding various amino acids (100 µM), inset: combine absorbance plot of active amino acid for sensing, and (b) UV-Vis titration curve of receptor in presence of sensor active amino acid D/ L-Trp (0-20 equiv.). Inset: magnified range of isosbestic point at λ~302 nm.

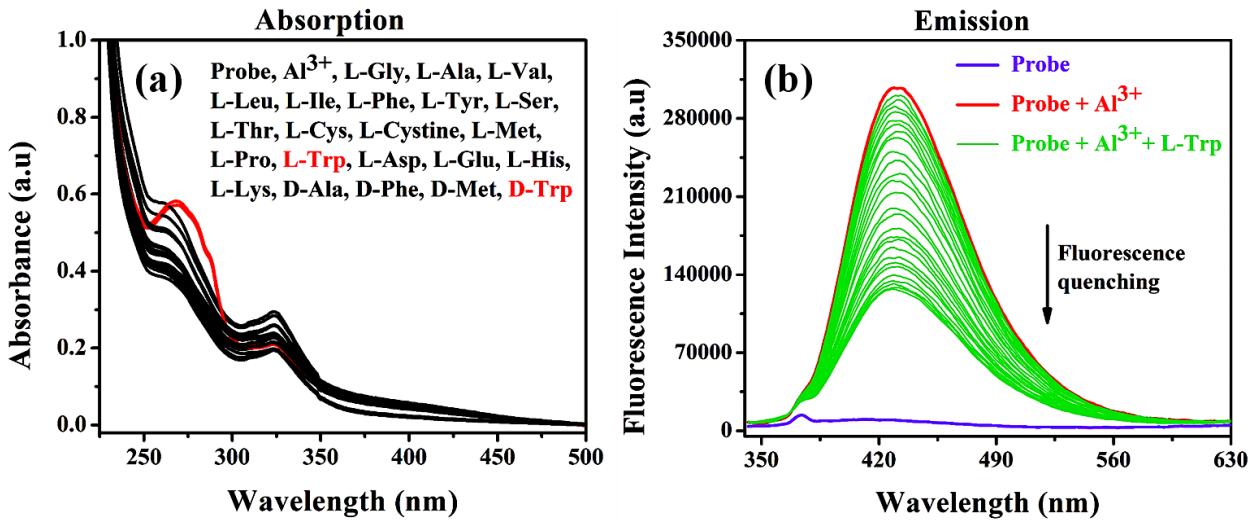

Fig. S8 (a) Absorption spectra of Al^{3+} complex in presence of various amino acids in water ([L] = 10 μM, [amino acid(s)] = 100 μM), (b) Fluorescence quenching in case of Al^{3+} complex upon addition of L-Trp ([L] = 10 μM, [M^{3+}] = 100 μM, [amino acid(s)] = up to 200 μM).

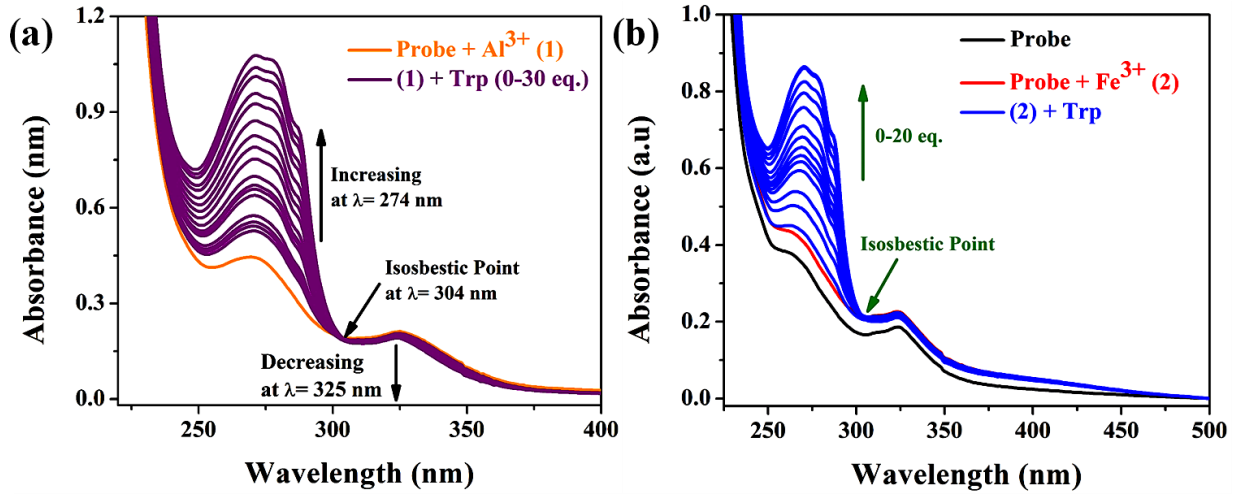

Fig. S9 L-Trp titration in presence of complexes (a) **1**, and (b) **2** showing isosbestic point ([L] = 10 μM, [M^{3+}] = 100 μM, [amino acid(s)] = up to 20 equiv. with respect to L).

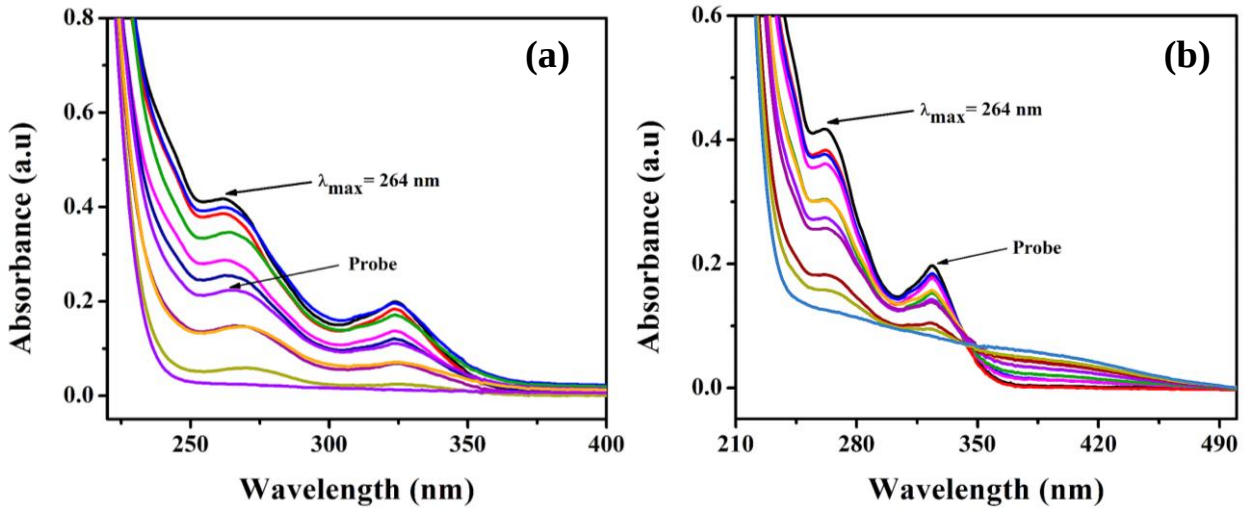

Fig. S10 Absorption spectra corresponding to the Jobs experiment of continuous variation of receptor **L** concentrations towards (a) Al^{3+}, and (b) Fe^{3+}.

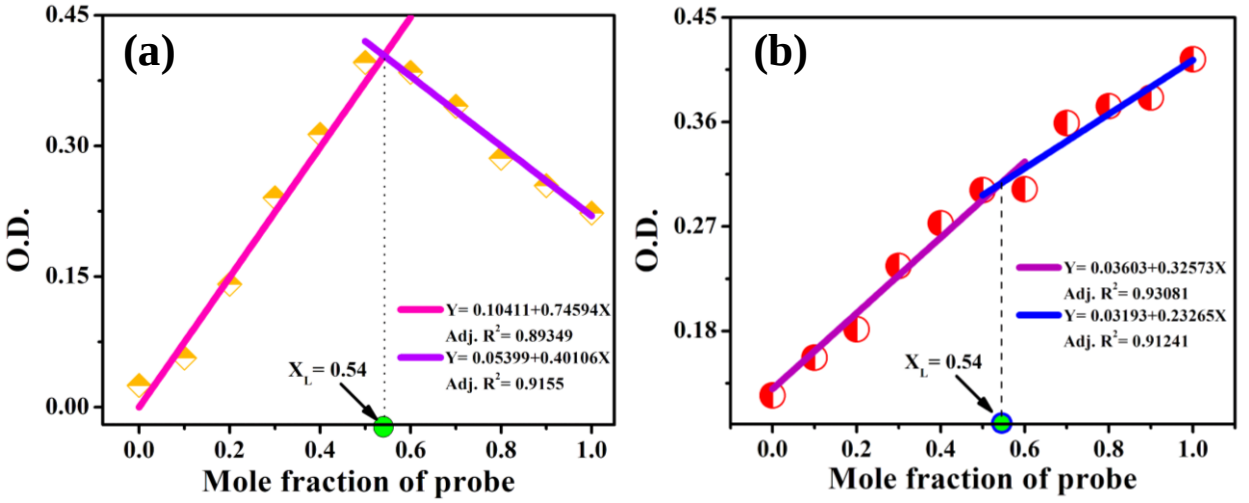

Fig. S11 Jobs plot for the determination of maximum binding affinity of probe **L** to the (a) Al^{3+}, (b) Fe^{3+} ions in water medium.

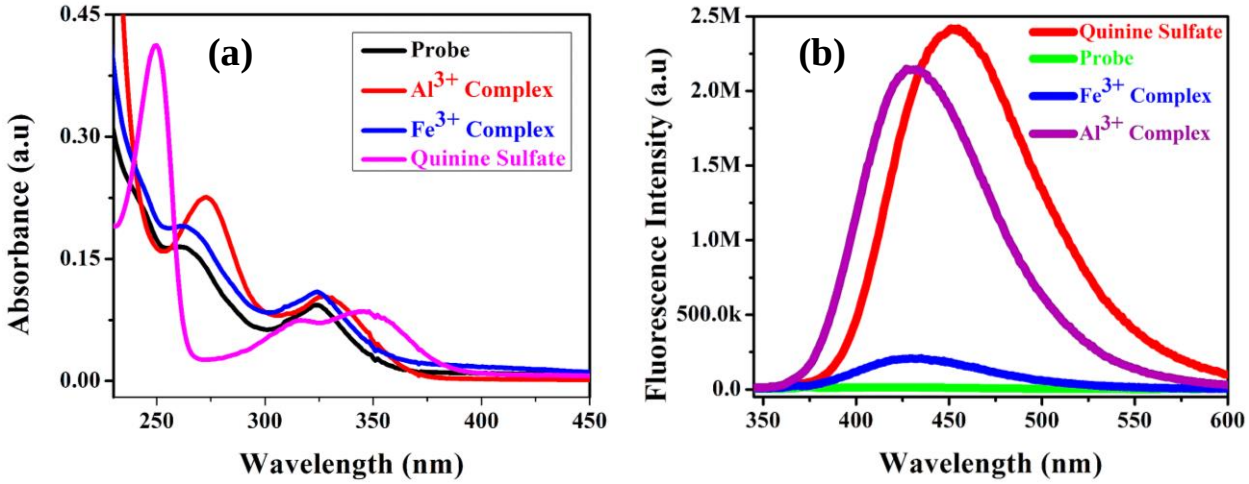

Fig. S12 Graphical representation for the determination of fluorescence quantum yield (Φ): (a) optical density (a.u.) of the receptor **L**, **L**+Al^{3+}, **L**+Fe^{3+} and quinine sulphate (QS) in water at 298 K; (b) corresponding emission intensity at λ_{ex} = 332 nm.

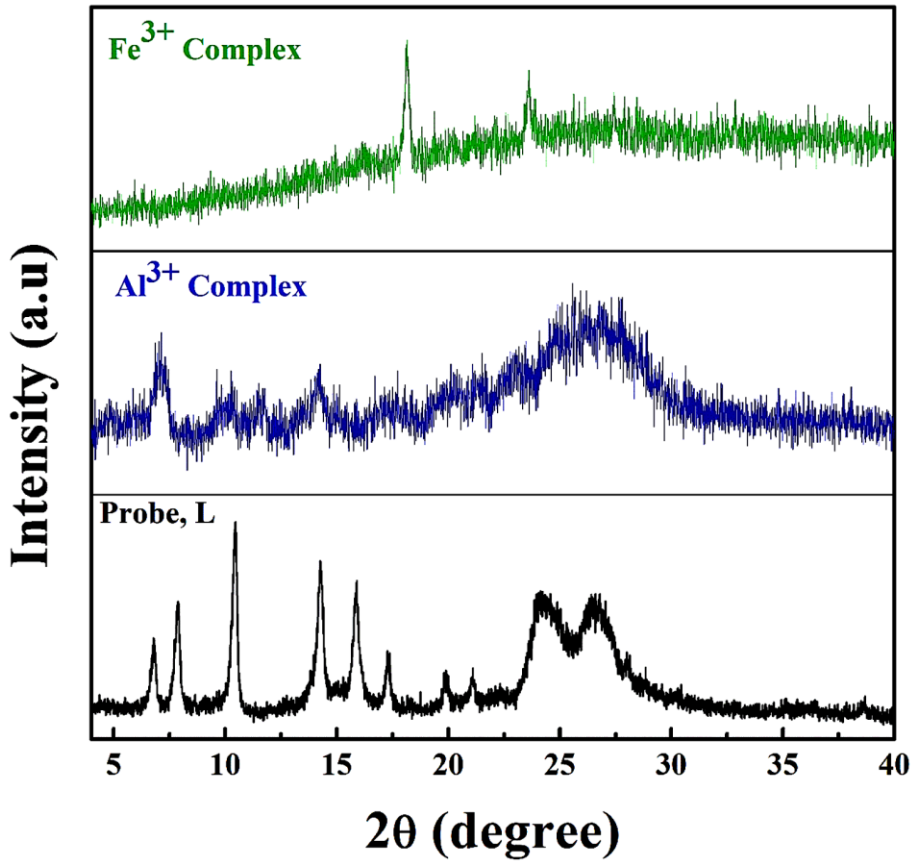

Fig. S13 PXRD data of probe **L** and its complexes.

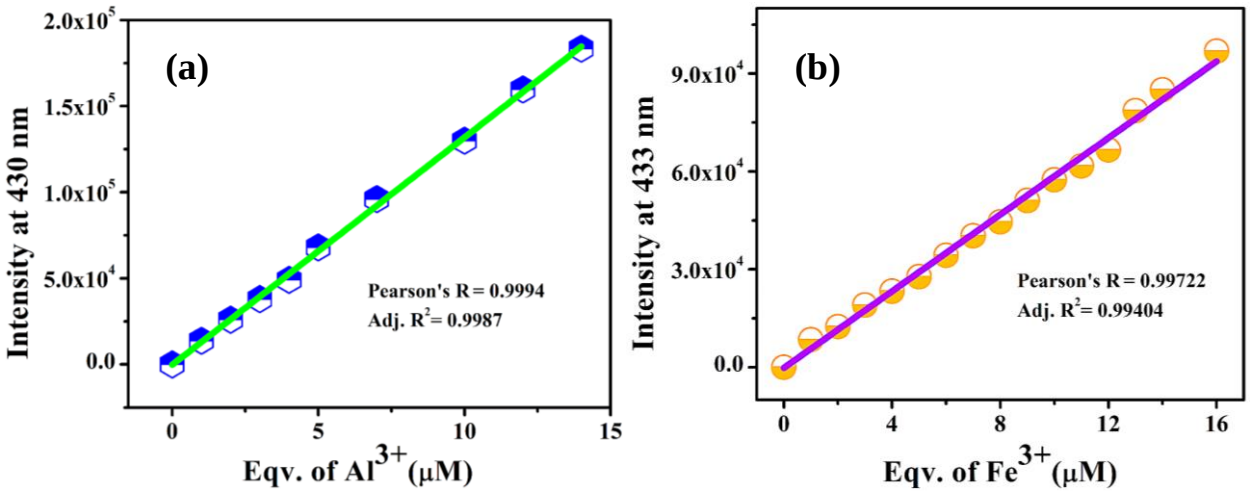

Fig. S14 Calculation of limit of detection (LOD) values in case of probe towards (a) Al^{3+} and (b) Fe^{3+} metal ions.

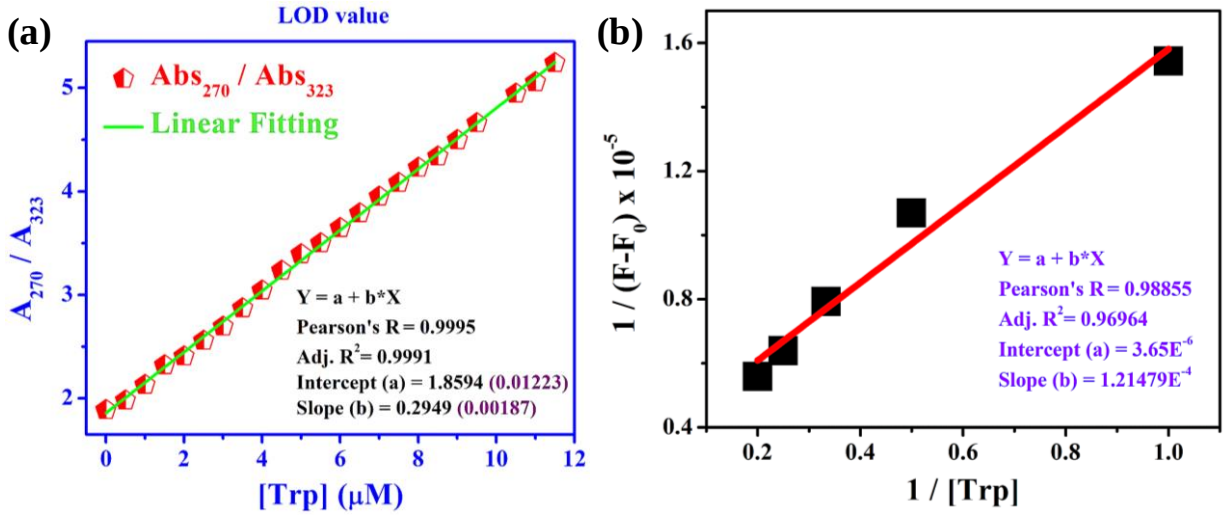

Fig. S15 (a) Calibration curve to determine the limit of detection of the receptor **L** for tryptophan amino acid (A: optical density at λ_{max} 270, and 323 nm). Digits in violet color represents the standard error values for the intercept, and slope, respectively. (b) Benesi-Hildebrand plot to determine the value of association constant (K_a) for Al^{3+} complex with L-Trp.

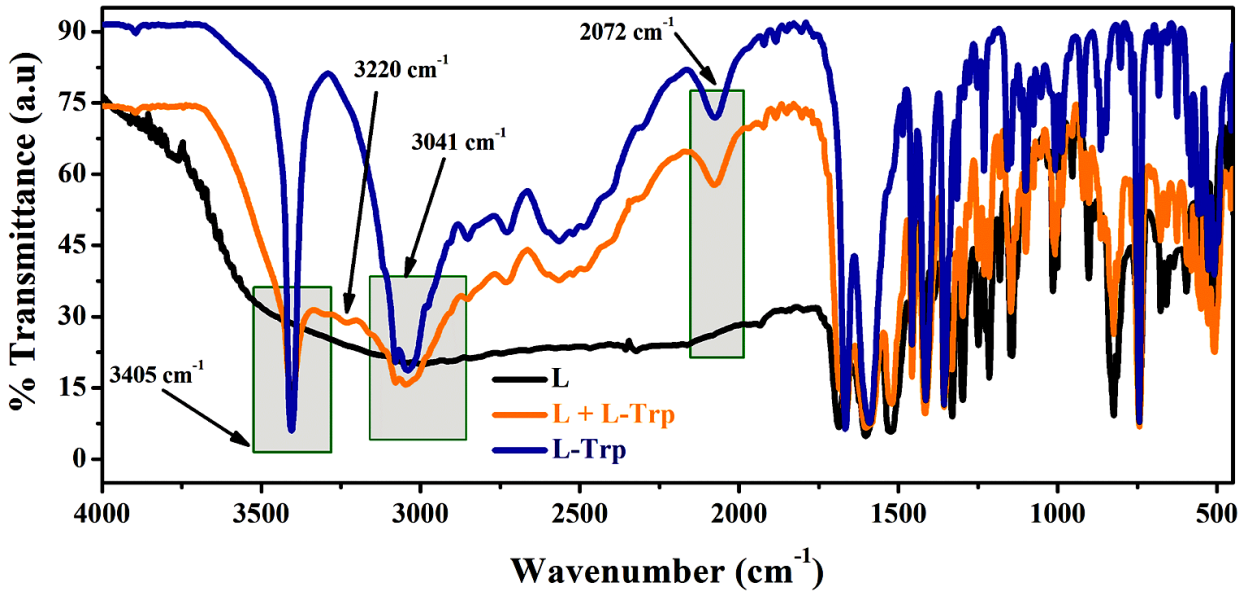

Fig. S16 FTIR spectral representation during L-Trp titration with probe **L** (υ in cm^{-1}).

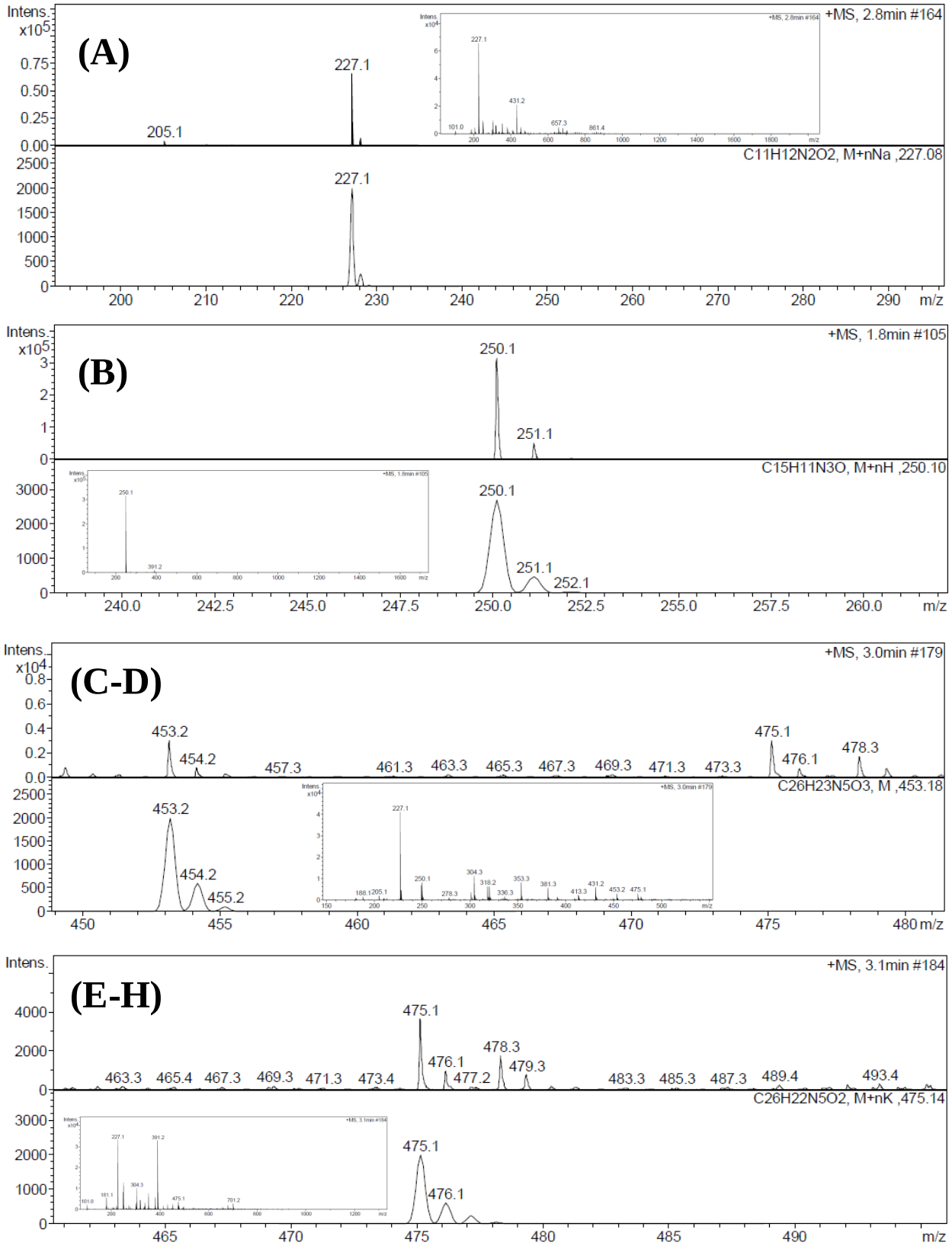

Fig. S17 ESI-MS data of the intermediates (C-H) formed during Pictet-Spengler reaction.

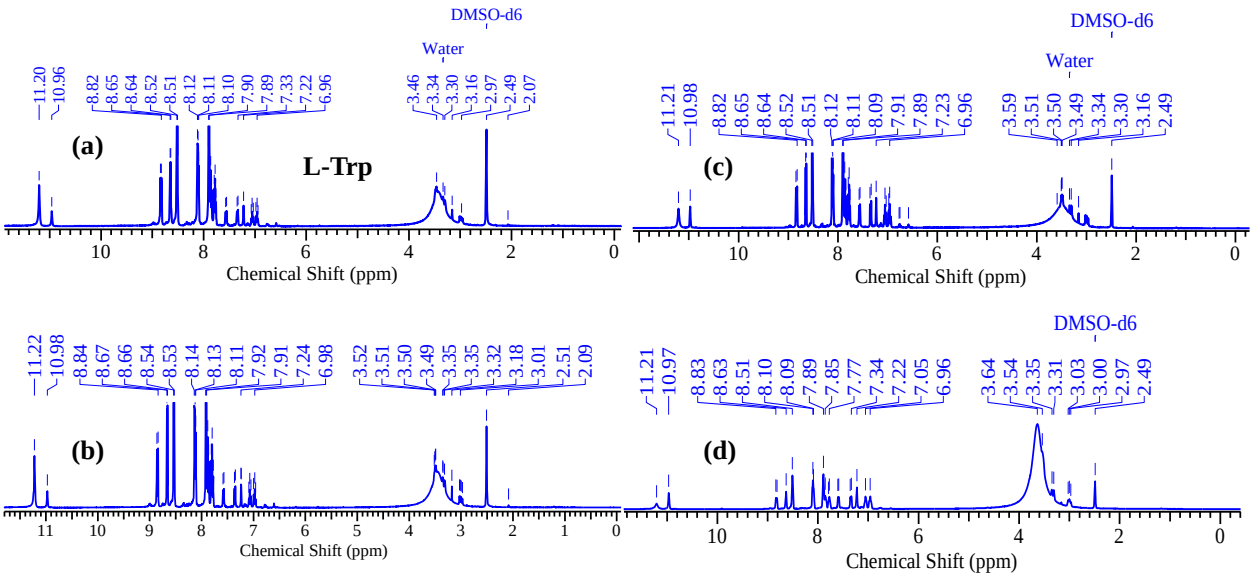

Fig. S18 ^{1}H NMR spectroscopy introducing (a) free amino acid, tryptophan, and (b-d) its reaction intermediates produced during the reaction with amide L.

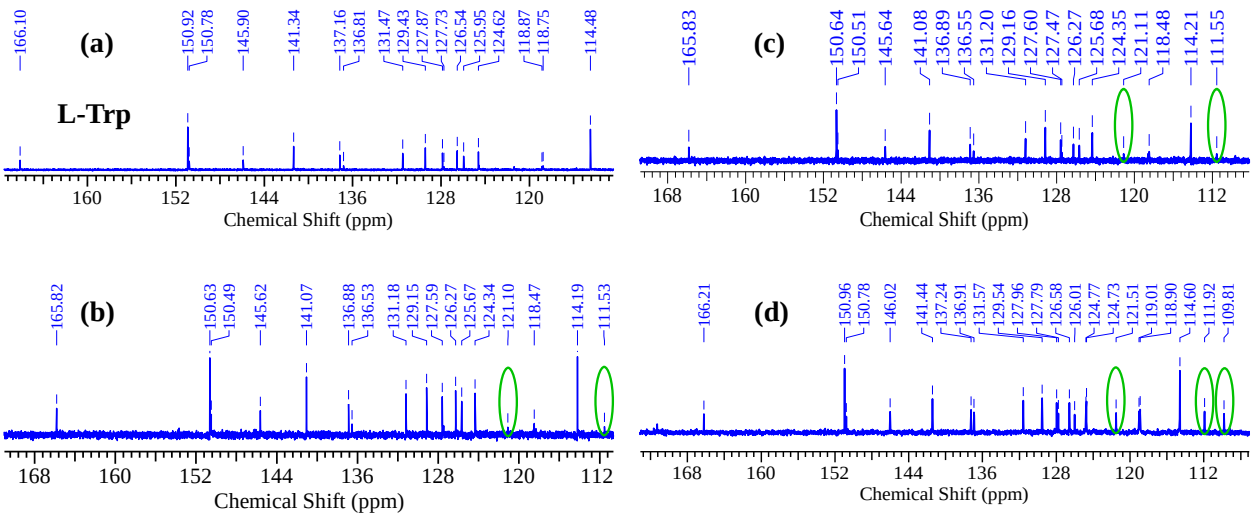

Fig. S19 ^{13}C NMR spectroscopy including (a) free amino acid, tryptophan, and (b-d) its reaction intermediates produced during the reaction with amide L.

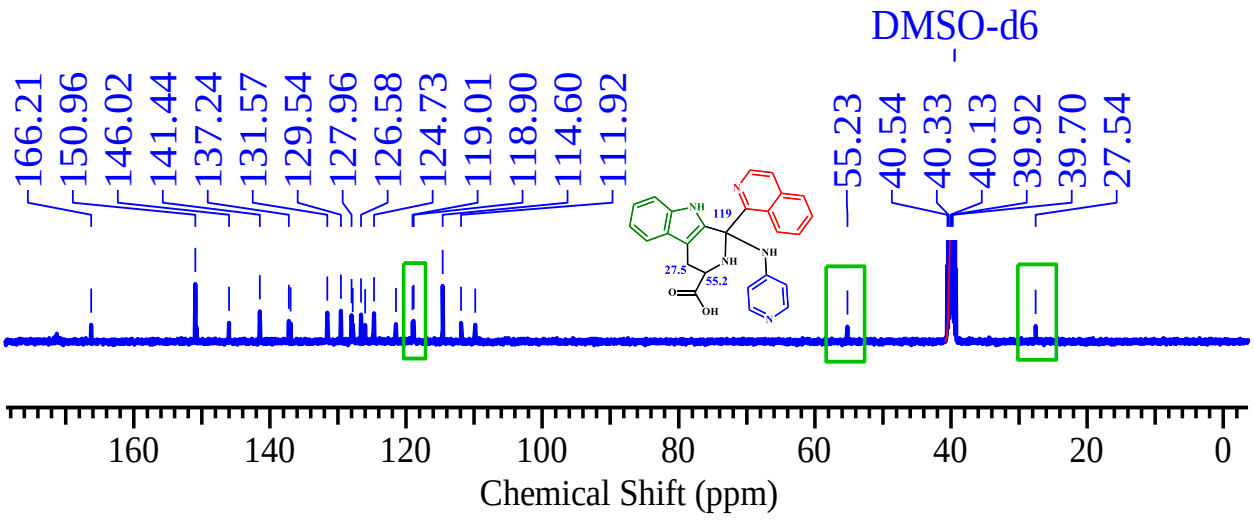

Fig. S20 Full range ^{13}C NMR spectroscopy of the cyclic Pictet-Spengler product 'H'.

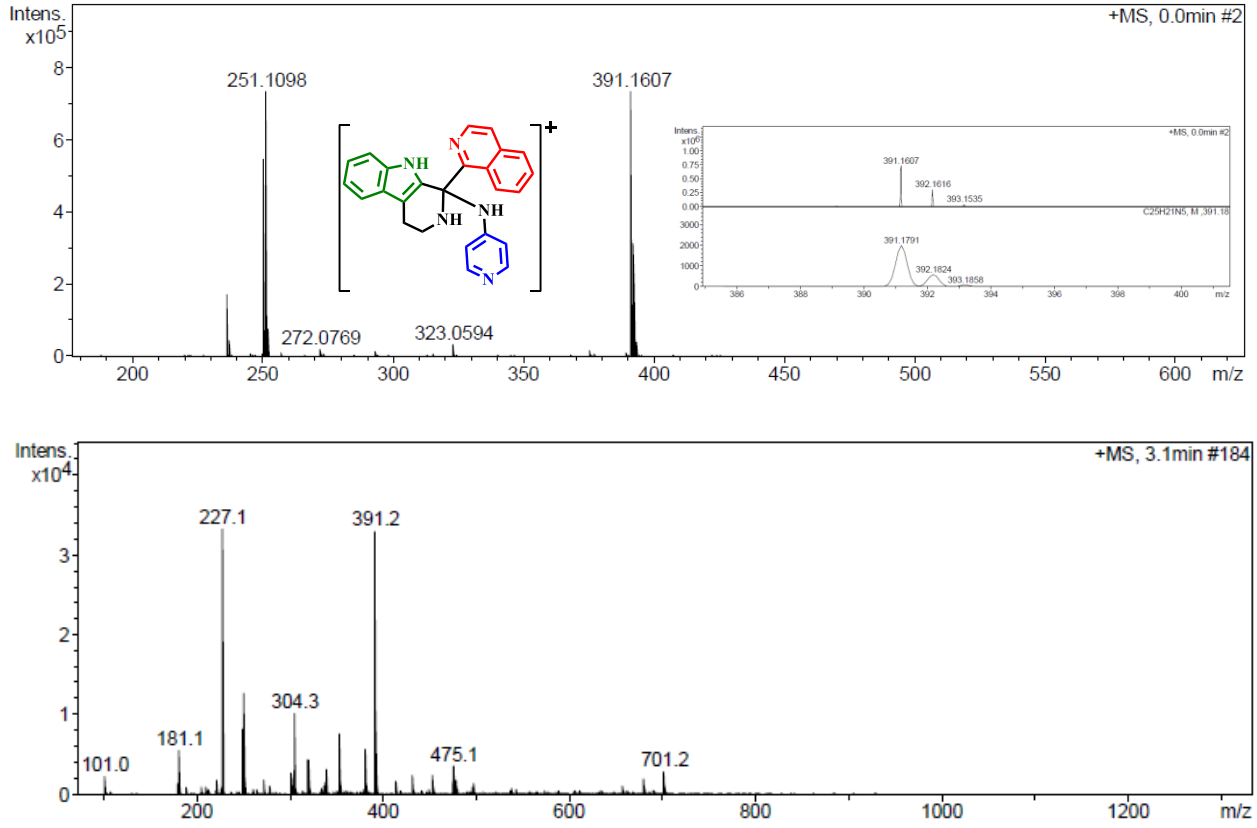

Fig. S21 ESI-MS data of the Pictet-Spengler product 'H' as per usual condition (top) and during sensing between **L** and Trp (bottom).

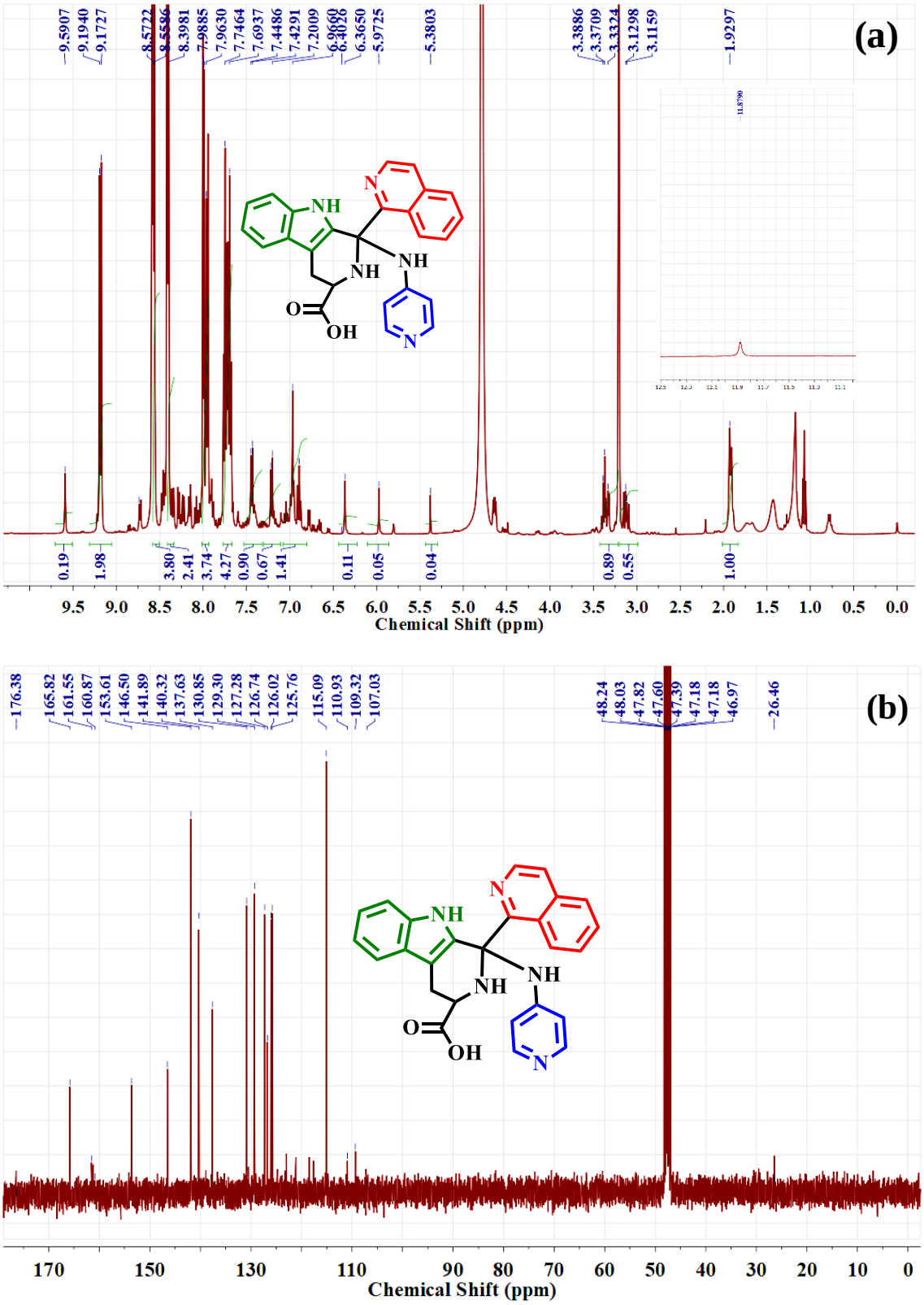

Fig. S22 Pictet-Spengler product 'H': (a) ^{1}H NMR, and (b) ^{13}C NMR.

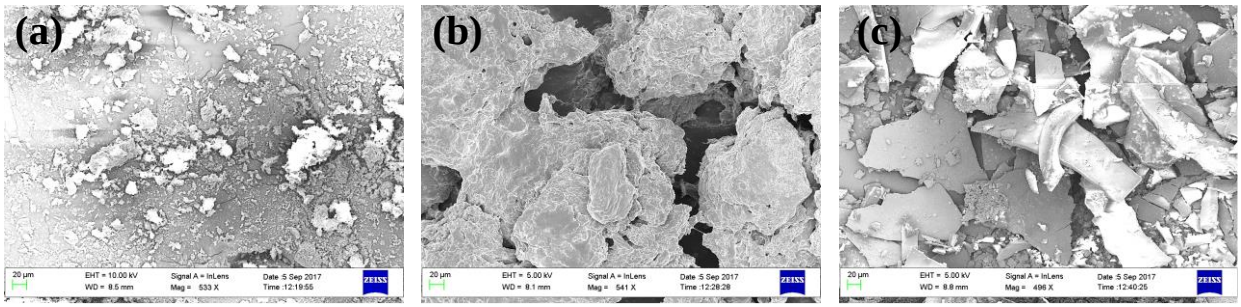

Fig. S23 FE-SEM images of (a) the probe **L** and its metal complexes: (b) Al^{3+} complex, and (c) Fe^{3+} complex in power form (Scale bar: 20 μm).

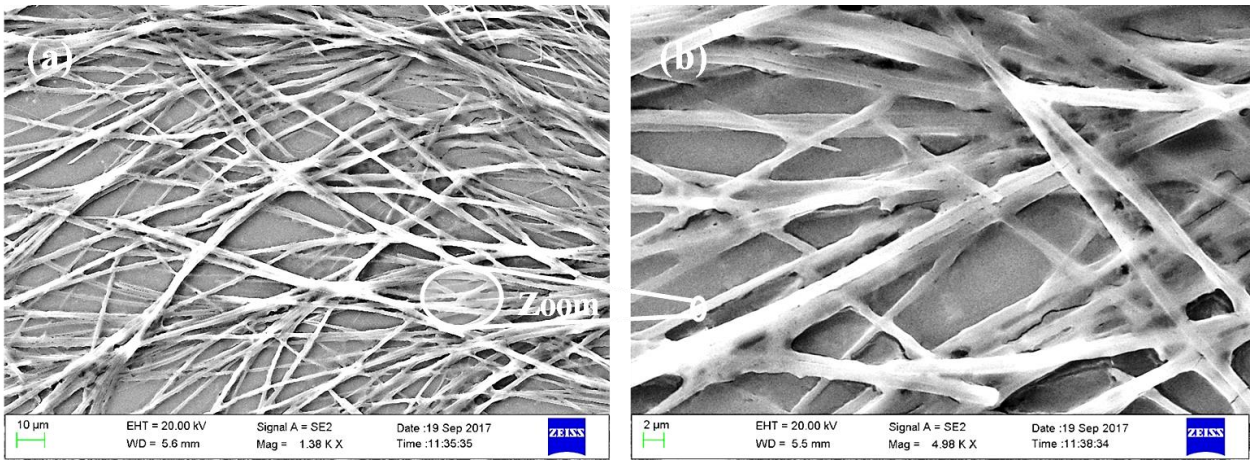

Fig. S24 Magnified SEM image of L-Trp in presence of Al^{3+} complex (Scale bar: (a) 10 μm, and (b) 2 μm).

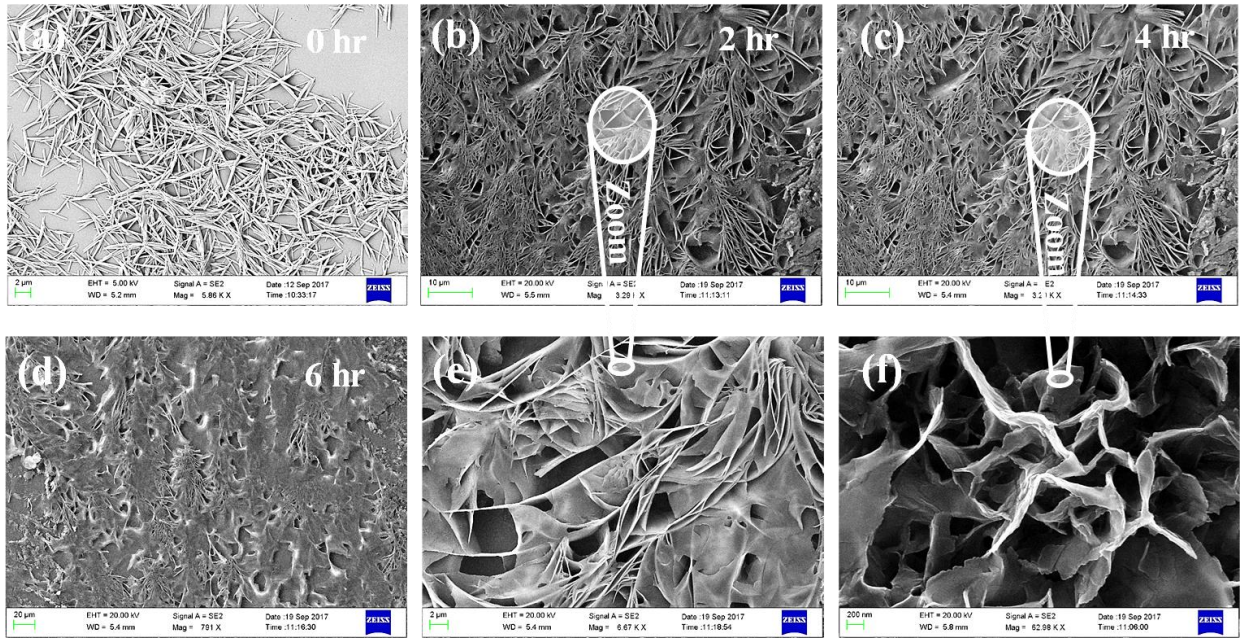

Fig. S25 Time dependent FE-SEM images of L-Tryptophan before and after addition of Fe^{3+} complex (Scale bar: (a) 2 μm, (b) 10 μm, (c) 10 μm, (d) 20 μm, (e) 2 μm, and (f) 200 nm).

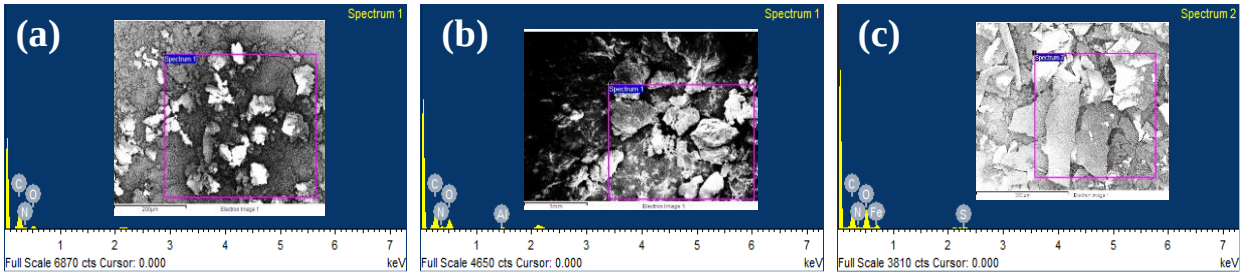

Fig. S26 EDAX analysis of (a) probe **L**, (b) Al^{3+} complex, and (c) Fe^{3+} complex.

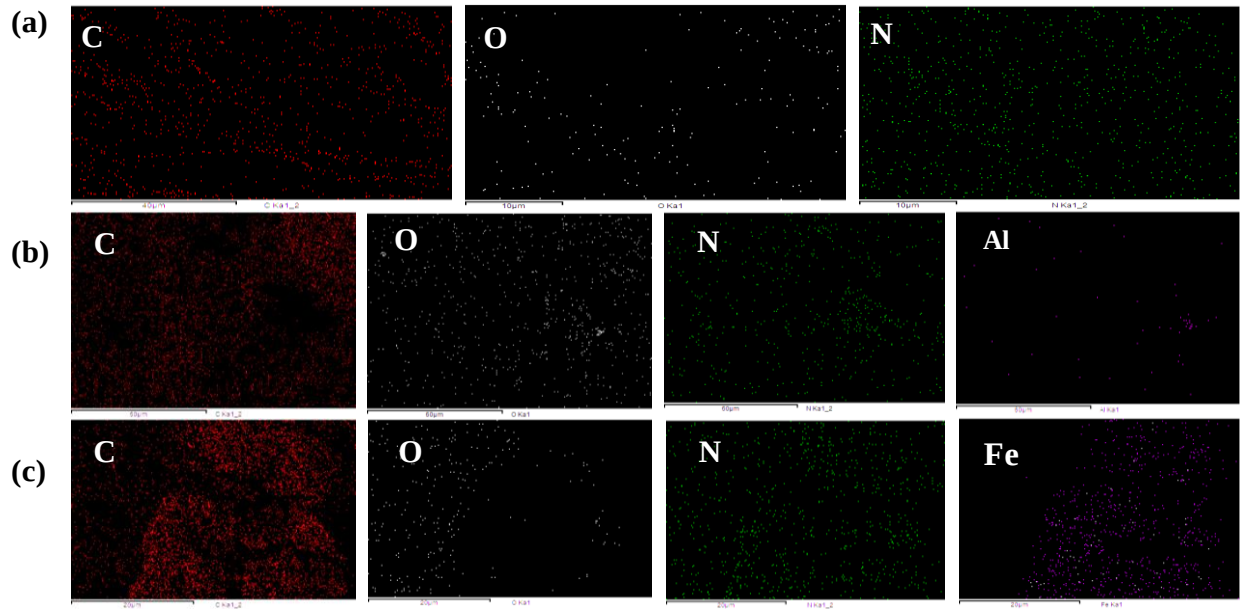

Fig. S27 Color mapping images of (a) probe **L**, (b) Al^{3+} complex, and (c) Fe^{3+} complex (metal nitrate salt was used to perform this experiment).

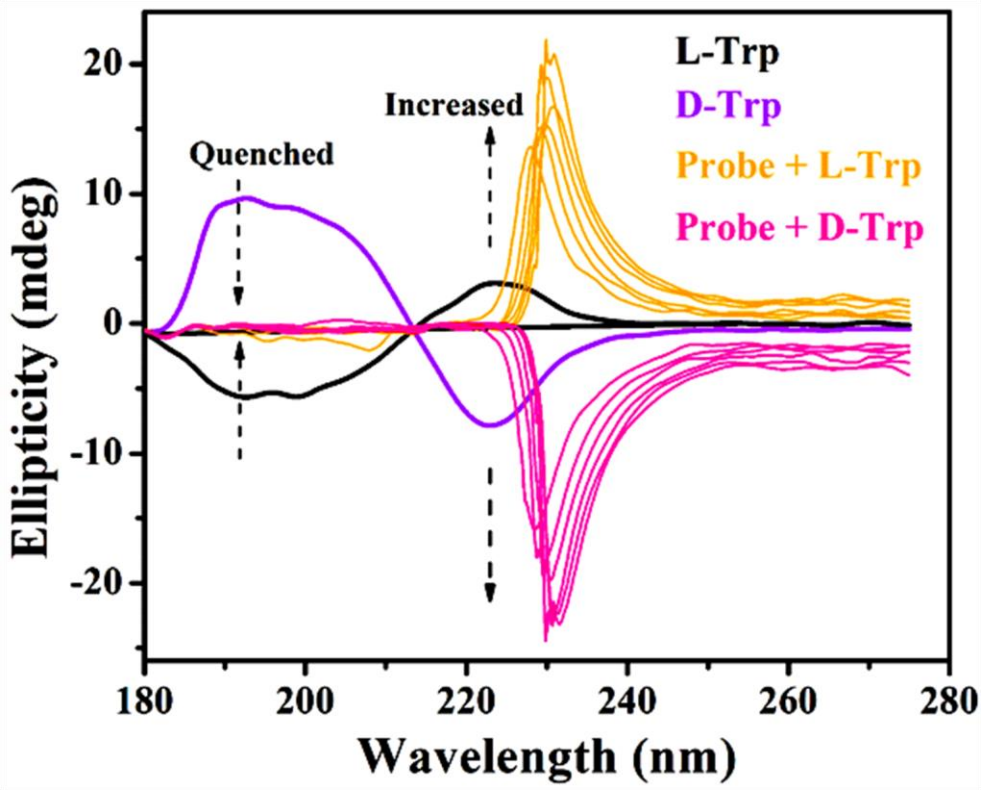

Fig. S28 Combine circular dichroism spectra of D/ L-Trp titration with probe L ([Trp] = 100 μM, [L] = 0-0.8 equiv.).

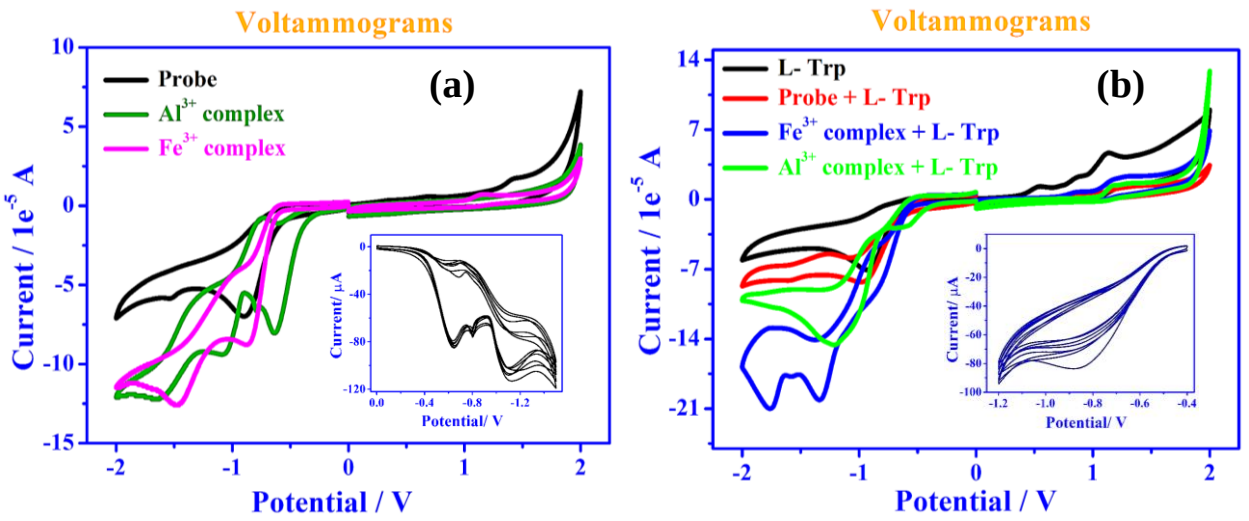

Fig. S29 Cyclic voltammograms of (a) probe **L** and its metal complexes, and (b) L-tryptophan with **L** and after consequent addition of metal ions. Inset: consecutive cycles under fixed condition (a) Al^{3+} complex, and (b) L-Trp. (Solvent = CH_3CN, scan rate = 100 mV/Sec, 0.1 mol L^{-1} $TBAPF_6$ as an electrolyte; glassy carbon as working electrode, Pt-wire counter electrode, and $Hg/HgCl_2$ reference electrode at 25 °C.)

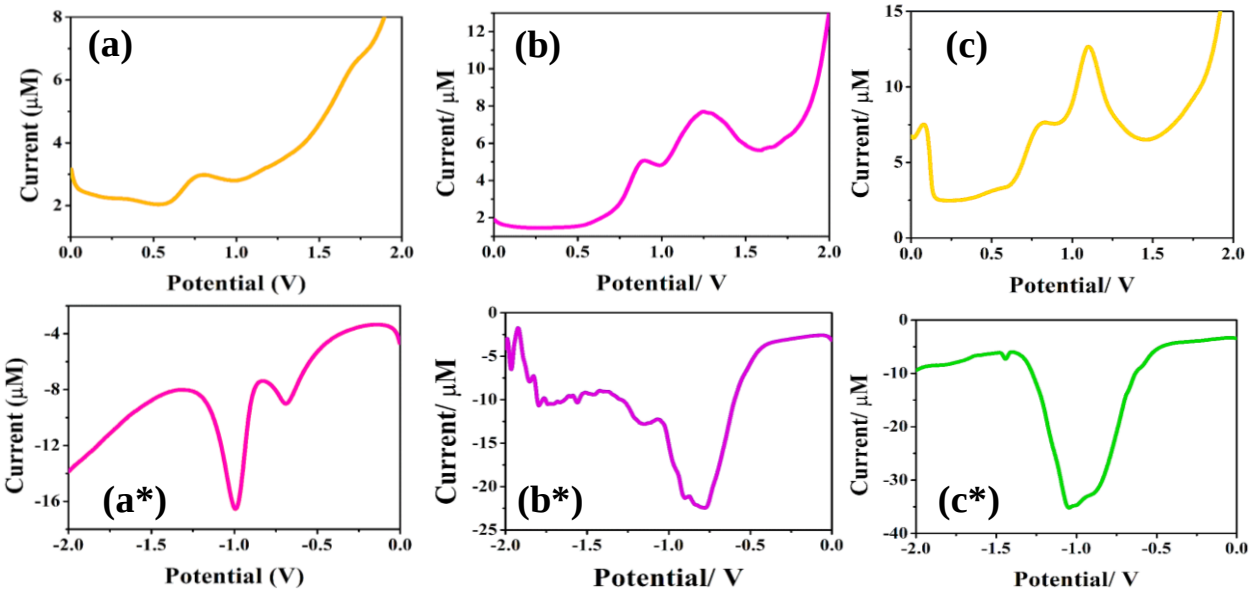

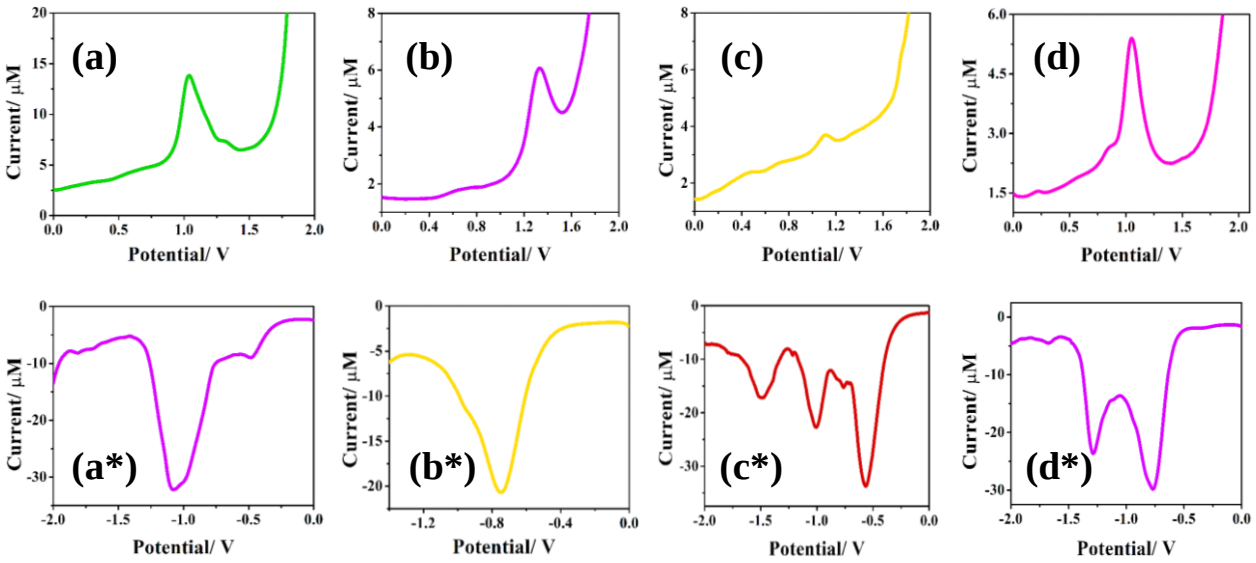

Fig. S30 Various range of differential pulse voltammograms of (top) probe and its metal complexes, and (bottom) complexation with D/ L-Trp showing oxidation and reduction peak potentials. * denotes the DPV curve in the cathodic zone.

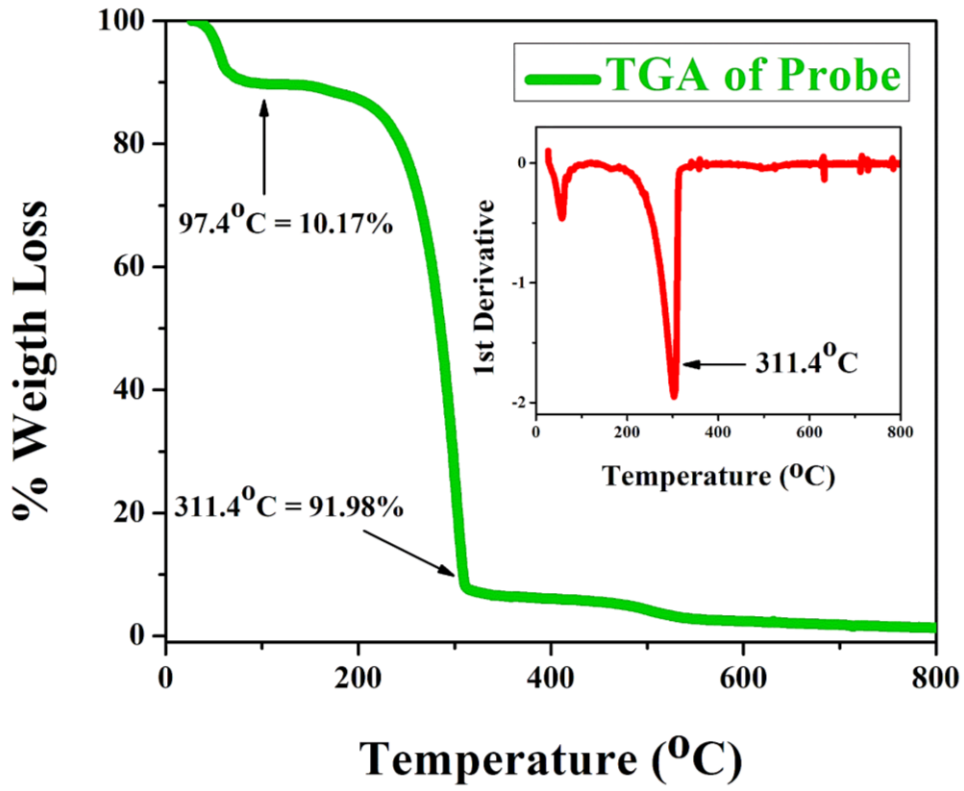

Fig. S31 Thermal stability (TGA) of probe **L**.

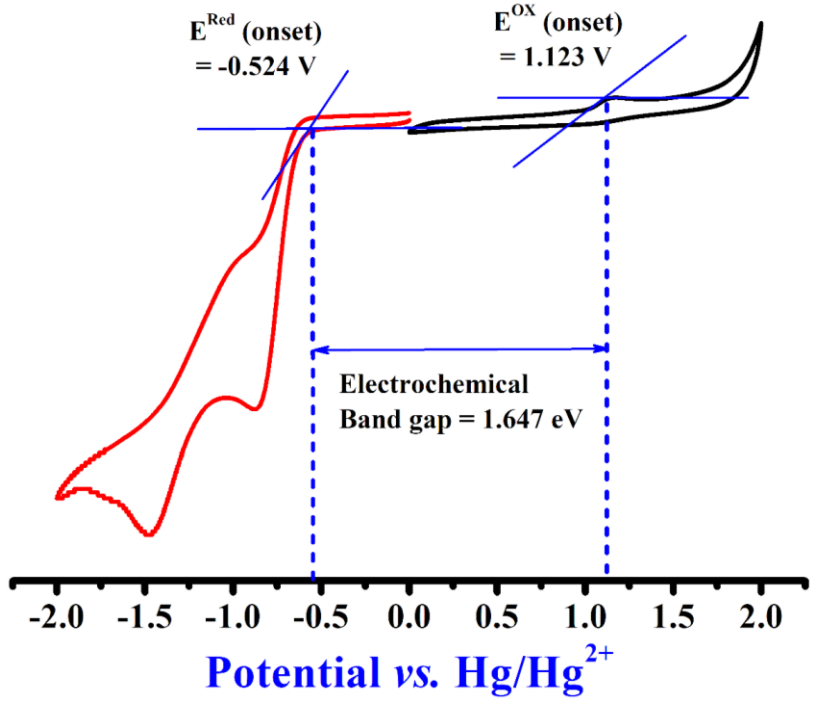

Fig. S32 Electrochemical energy gap of Fe^{3+} complex[12]

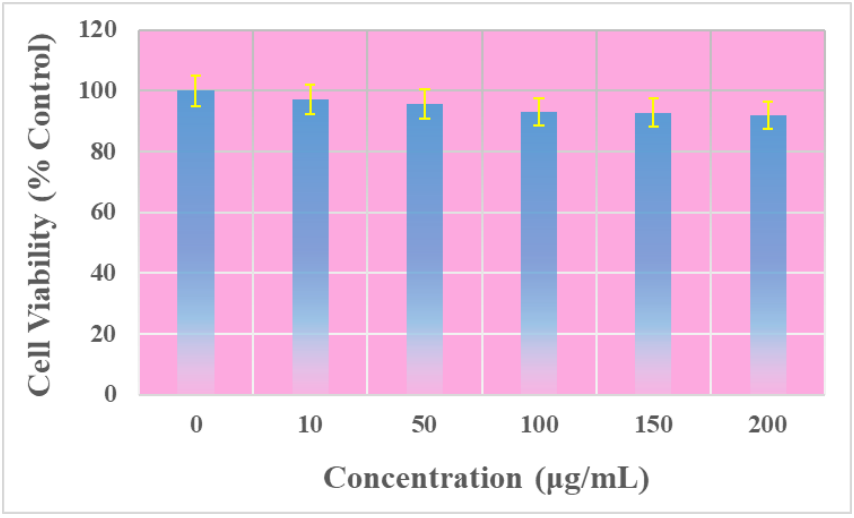

Fig. S33 Cell redox activity plot of Al(III)-complex using HeLa cell line through MTT assay.

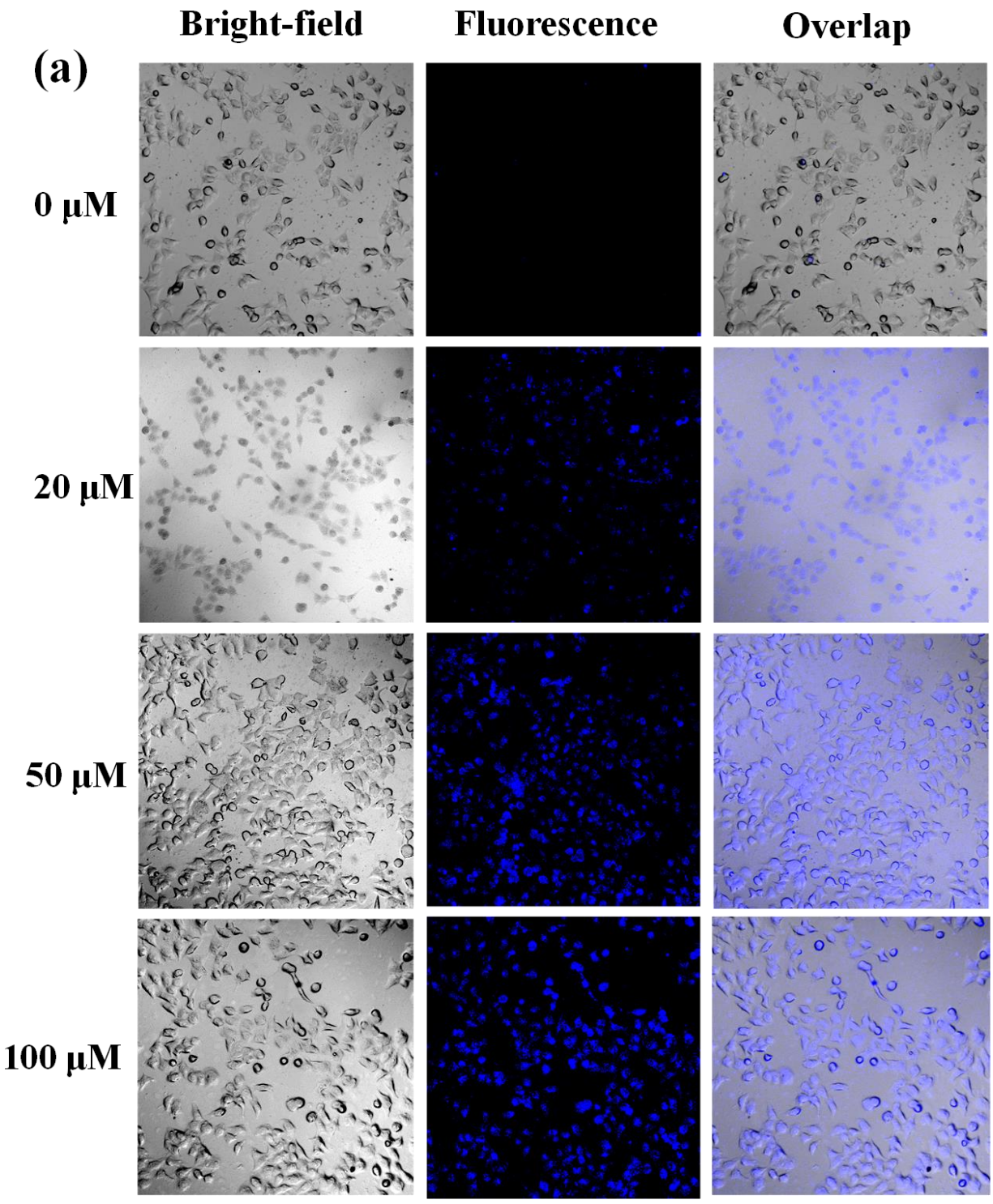
(a)
Bright-field
Fluorescence
Overlap
0 μM
20 μM
50 μM
100 μM

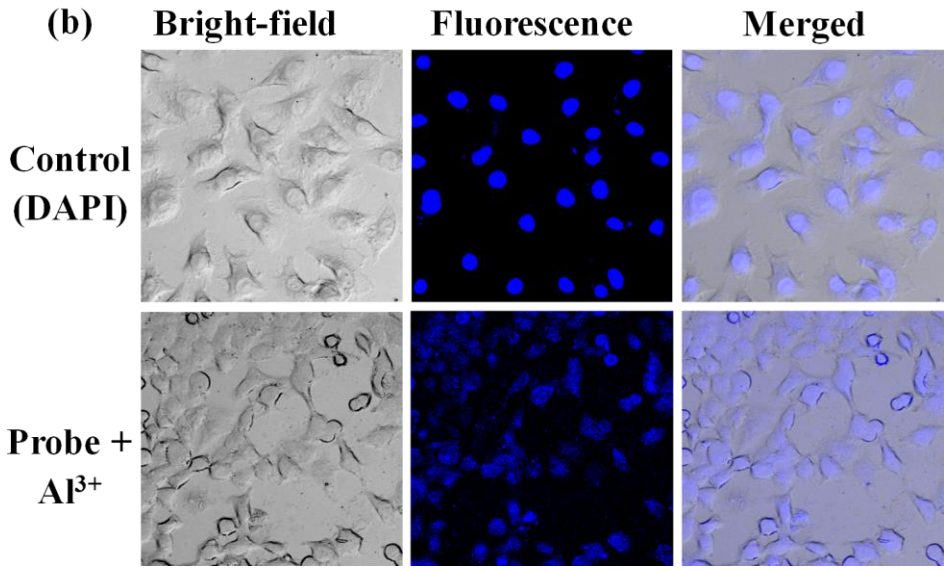

Fig. S34 Confocal microscopic fluorescence images of HeLa cells: (a) variation in concentrations of compound (0, 20, 50, and 100 μg/mL); (b) corresponding zoom images in presence of control and compound.

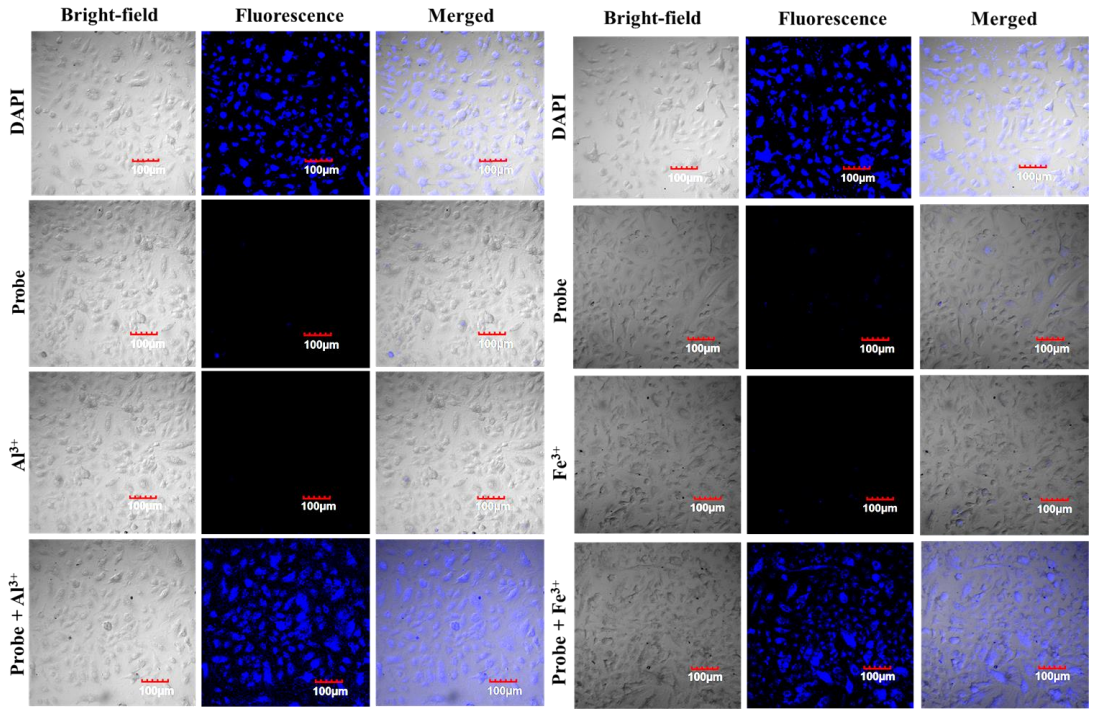

Fig. S35 Confocal microscopic images in a549 cell lines of control (100 ng/mL), probe, Al^{3+}, Fe^{3+}, Al^{III}, and Fe^{III}-complex (100 μg/mL) in bright-field and UV laser (blue, laser wavelength of 405 nm) filters.

Scheme S1. Synthesis of receptor L and corresponding metal sensors.

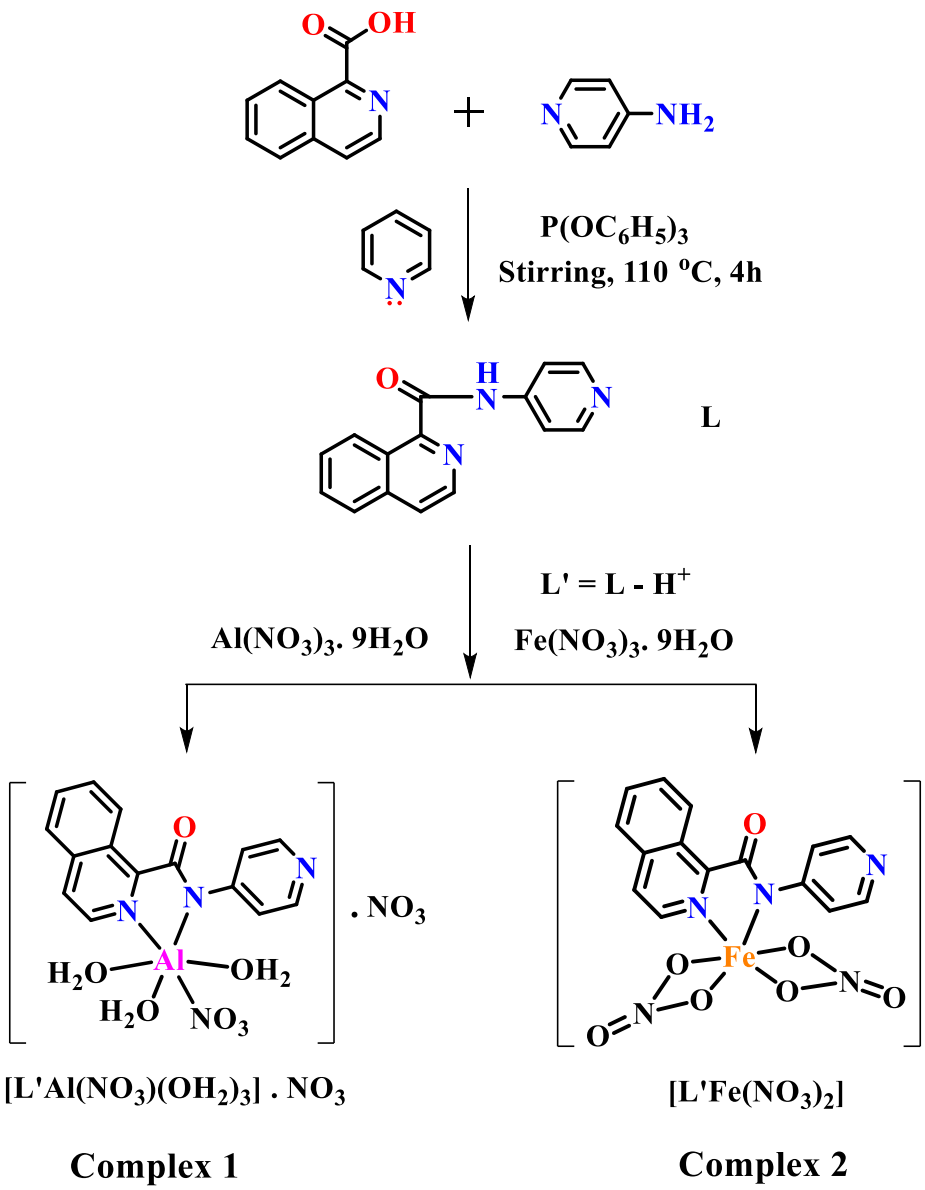

Scheme S2. Probable mechanism for the Pictet-Spengler reaction of amide **L**, and L-Trp.

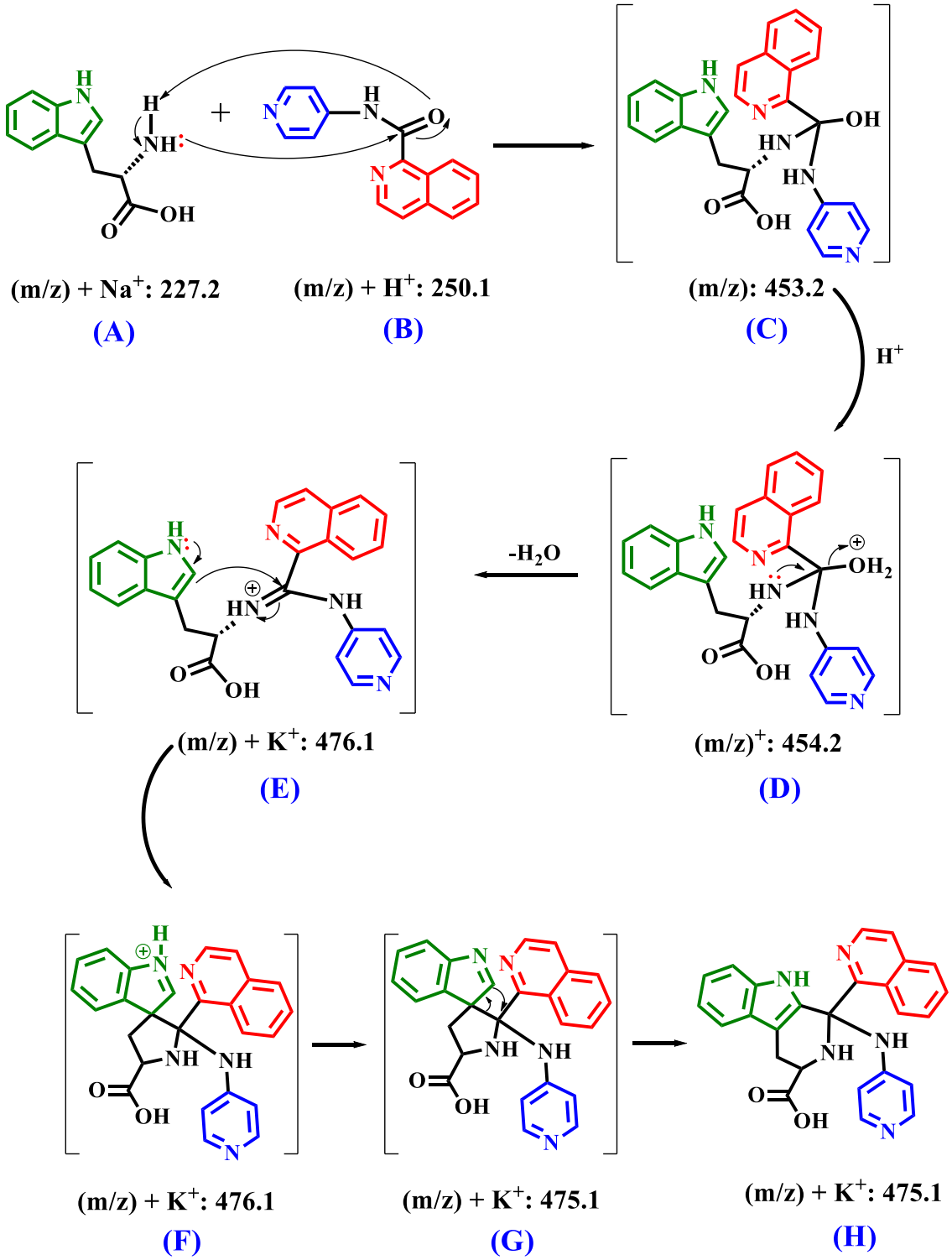

Scheme S3. General representation of PET based mechanism for **L**–Al^{3+} sensor system.

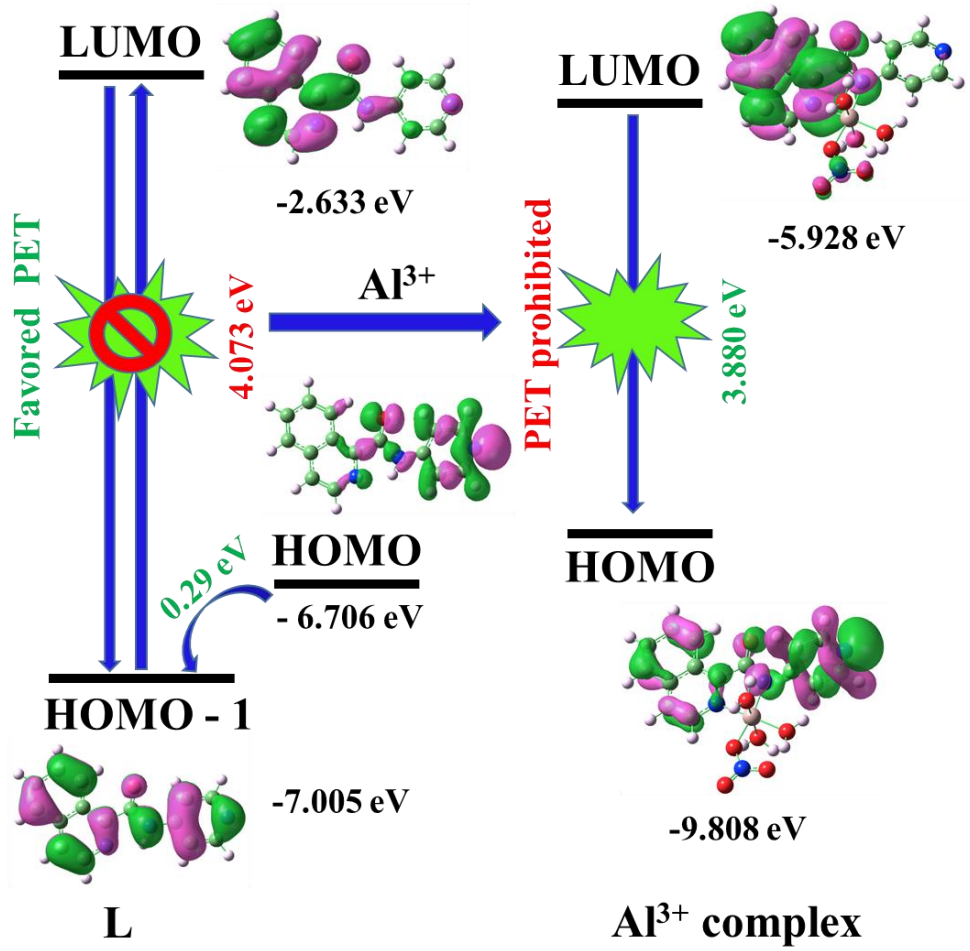

Scheme S4. Plausible quenching mechanism of **L**+M^{3+} in presence of L-Trp or BSA.

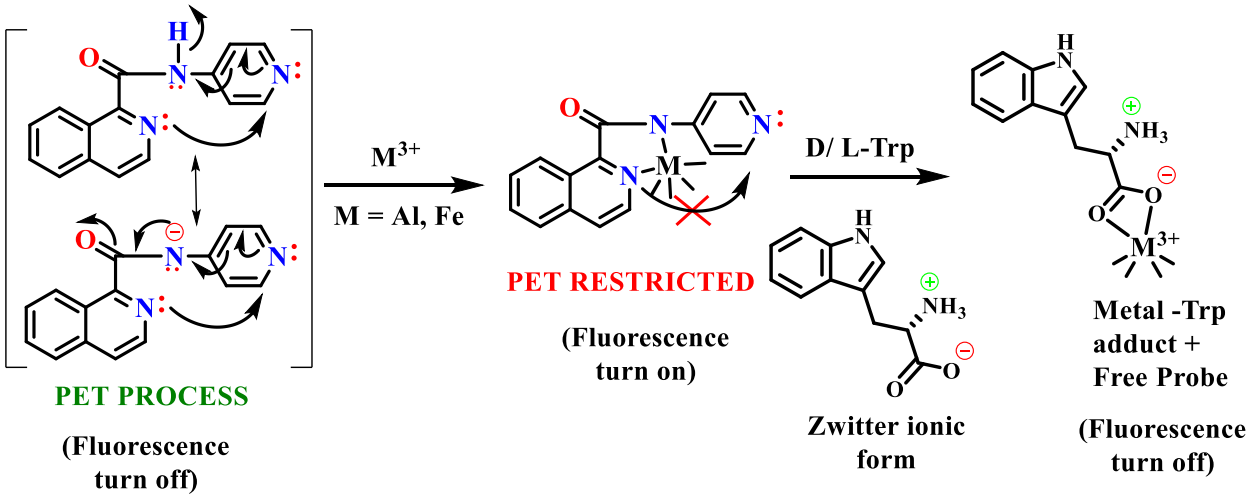

Table S1. Experimental infrared absorption frequencies (cm^{-1}) of free ligand and in presence of metal ions as well as amino acid (L-Trp). (Assignment of band frequencies to bond vibrational modes)

Ligand/ Complex	*Bond vibrational modes (Stretching-υ). Band position (cm^{-1})*					
	C=O	***C=N***	***N-H***	***N-O***	***M-O***	***M-N***
L	1762	1516, 1678	1511, 1600, 3667	-	-	-
Al^{3+} complex	1705	1626	1532, 3610	1479	537	496
Fe^{3+} complex	1700	1637	1527, 3615	1490	542	506
L-Trp	1665	-	1519, 1608, 3405	-	-	-
L + L-Trp	1685	1512, 1589	3220	-	-	-

Table S2. Comparisons of binding constant, and LOD of various Trp based sensors

Entry	*Probe*	*λ_{ex}/ λ_{em} (nm)*	*K_a/ K_d*	*LOD*	*Ref.*
1	Ru(II) complex **1**	280/ 313	$3.0 \times 10^4\ M^{-1}$	300 nM	[13]
2	Ru(II) complex **2**	308/ 355	$2.1 \times 10^3\ M^{-1}$	300 nM	[14]
3	8-(Alkoxy)quinoline-based fluorescent probe	280/ 342	$6.4 \times 10^4\ M^{-1}$	-	[15]
4	Amphiphilic fluorophore	275/ 334	$3.4 \times 10^5\ M^{-1}$	-	[16]
5	$[Pt(bzimpy)Cl]^+$	-	$6.7 \times 10^4\ M^{-1}$	-	[17]
6	SQ	280/ 340	$1.4 \times 10^6\ M^{-1}$	-	[18]
7	MMAPA	As per BSA	$6.3 \times 10^4\ M^{-1}$	-	[19]
8	Co(II) complex **1**	290/ 340	$1.7 \times 10^3\ M^{-1}$	56 nm	[20]
9	Amide probe **L**	332/ 430	$3.0 \times 10^5\ M^{-1}$	243 nm	*

*present work

Table S3. Wavelength maxima of L-tryptophan and its complexes in presence of probe **L**, and Al^{3+}/ Fe^{3+} adduct.

Entry	*Compound*	*λ_{max} on CD Spectra*
01	D/ L-Trp	223, 192 nm
02	D/ L-Trp + Receptor L	221, 202 nm
03	D/ L-Trp + Al^{3+} complex	224 nm
04	D/ L-Trp + Fe^{3+} complex	225 nm

Table S4: Comparison of Cyclic Voltammograms of probe **L** before and after addition of M^{3+} (M= Al and Fe) and L-Trp in CH_3CN. (Scan Rate = 100 mV/Sec, 0.1 mol L^{-1} $TBAPF_6$ as an electrolyte; Pt-wire Counter electrode, Glassy carbon working electrode and $Hg/HgCl_2$ reference electrode at 25 °C.)

Entry	E_{red} / V			E_{ox} / V		
	E_{pc}	E_{pa}	$E_{1/2}$	E_{pc}	E_{pa}	$E_{1/2}$
Probe L	-0.75	-0.65	-0.70	-	+1.32, +0.69	-
Al^{3+} complex (1)	-0.57, -1.07	- 0.73, -1.43	- 0.65	-	+1.10, +0.48	-
Fe^{3+} complex (2)	-0.78, -1.28	- 0.99	- 0.88	-	+1.09, +0.85	-
L-Trp	-0.99	- 0.68	- 0.83	+ 1.04	+0.54, +0.87, +1.10	+ 1.07
L-Trp + L	-0.99, -0.28	-0.45, -1.27,	- 1.13	+ 0.88	+ 1.25	+ 1.06
L-Trp + (1)	-0.61, -1.21	-0.53	- 0.57	-	+ 1.15	-
L-Trp + (2)	-0.91, -1.32	-0.85, -1.73	- 0.88	+ 1.02	+0.84, + 1.24	+0.93

Table S5. DFT results and UV-Vis interpretation of **L** and its sensor active complexes.

Entry	**E[a] (Hartrees)**	**HOMO[b] (eV)**	**LUMO[b] (eV)**	**ΔE[b] (eV)**	**λ_{ex}[c] (nm)**		**Φ_f[d]**	**λ_{em}[e] (nm)**
					Thr.	Exp.		
Probe	-817.93865	-6.706	-2.633	4.073	340	332	0.313	401- 433
					245	242	0.535	
Al^{3+} complex	-1569.2018	-9.808	-5.928	3.880	357	332	0.321	405- 425
					276	276	0.139	
Fe^{3+} complex	-2641.1858	-10.528	-9.0393	1.488		333		445- 450
						275		

[a] Total energy (a.u.)

[b] HOMO, LUMO and HOMO-LUMO gaps are calculated with B3LYP/631G+(d,p)

[c] Theoritical and experimental excitation absorption maximum (nm)

[d] Quantum yield (Φ_f of standard Quinine Sulphate = 0.54 in water)

[e] Experimental emission wavelength maximum (nm)

Table S6. Summary of excitation energies and oscillator strengths.

Entry	Important orbital excitations	Oscillator strength (f)	Energy (eV)	% C	Wavelength (nm)	
					$\lambda_{thr.}$	$\lambda_{exp.}$
Probe	1. HOMO → LUMO	0.3132	3.6450	69.9	340	332
	2. HOMO - 4 → LUMO 3. HOMO - 2 → LUMO	0.0003	3.7405	37.6 58.8	331	
	4. HOMO - 3 → LUMO	0.0054	4.4949	69.2	275	270
	5. HOMO - 7 → LUMO 6. HOMO - 5 → LUMO 7. HOMO - 1 → LUMO + 1 8. HOMO → LUMO + 1 9. HOMO → LUMO + 2	0.5346	5.0406	10.9 27.9 13.6 46.8 39.1	245	242
Al^{3+} complex	1. HOMO → LUMO + 1 2. HOMO → LUMO + 2	0.3212	3.4693	35.5 60.2	357	333
	3. HOMO - 6 → LUMO 4. HOMO - 6 → LUMO + 3 5. HOMO - 5 → LUMO + 3 6. HOMO - 3 → LUMO + 2 7. HOMO - 2 → LUMO + 2 8. HOMO - 1 → LUMO + 2 9. HOMO → LUMO + 4	0.1161	4.3343	11.2 34.9 11.4 21.3 10.4 50.2 10.6	286	275
	10. HOMO - 3 → LUMO + 1 11. HOMO - 3 → LUMO + 2 12. HOMO → LUMO + 3	0.1394	4.4768	13.2 24.3 62.4	276	

References:

1. I. D. Kuntz, F. P. Gasparro, M. D. Johnston and R. P. Taylor, *Journal of the American Chemical Society*, 1968, 90, 4778-4781.
2. Y. Upadhyay, T. Anand, L. T. Babu, P. Paira, A. Kumar Sk, R. Kumar and S. K. Sahoo, *Journal of Photochemistry and Photobiology A: Chemistry*, 2018, 361, 34-40.
3. L. Ismail and M. Abdel-Mottaleb, *International Journal of Photoenergy*, 2003, 5, 249-254.
4. B. K. Kundu, P. Mandal, B. G. Mukhopadhyay, R. Tiwari, D. Nayak, R. Ganguly and S. Mukhopadhyay, *Sensors and Actuators B: Chemical*, 2019, 282, 347-358.
5. T. Yanai, D. P. Tew and N. C. Handy, *Chemical Physics Letters*, 2004, 393, 51-57.
6. A. Kuwar, R. Patil, A. Singh, S. K. Sahoo, J. Marek and N. Singh, *Journal of Materials Chemistry C*, 2015, 3, 453-460.
7. D. Jacquemin, E. A. Perpete, G. E. Scuseria, I. Ciofini and C. Adamo, *Journal of chemical theory and computation*, 2008, 4, 123-135.
8. M. Das, B. Kumar Kundu, R. Tiwari, P. Mandal, D. Nayak, R. Ganguly and S. Mukhopadhyay, *Inorganica Chimica Acta*, 2018, 469, 111-122.
9. P. Mandal, B. K. Kundu, K. Vyas, V. Sabu, A. Helen, S. S. Dhankhar, C. M. Nagaraja, D. Bhattacherjee, K. P. Bhabak and S. Mukhopadhyay, *Dalton Transactions*, 2018, 47, 517-527.
10. P. Mandal, N. Malviya, K. Kundu Bidyut, S. Dhankhar Sandeep, C. M. Nagaraja and S. Mukhopadhyay, *Applied Organometallic Chemistry*, 2017, 32, e4179.
11. B. Kumar Kundu, V. Chhabra, N. Malviya, R. Ganguly, G. S. Mishra and S. Mukhopadhyay, *Microporous and Mesoporous Materials*, 2018, 271, 100-117.
12. Y. Rout, P. Gautam and R. Misra, *The Journal of Organic Chemistry*, 2017, 82, 6840-6845.
13. P. R. Callis, in *Methods in enzymology*, Elsevier, 1997, vol. 278, pp. 113-150.
14. P. R. Callis and B. K. Burgess, *The Journal of Physical Chemistry B*, 1997, 101, 9429-9432.
15. H. Shizuka, M. Serizawa, T. Shimo, I. Saito and T. Matsuura, *Journal of the American Chemical Society*, 1988, 110, 1930-1934.
16. B. Alpert, M. Jameson David and G. Weber, *Photochemistry and Photobiology*, 1980, 31, 1-4.
17. R. E. Dickerson and I. Geis, *Hemoglobin: structure, function, evolution, and pathology*, Benjamin-Cummings Publishing Company, 1983.
18. N. Tayeh, T. Rungassamy and J. R. Albani, *Journal of Pharmaceutical and Biomedical Analysis*, 2009, 50, 107-116.
19. X. M. He and D. C. Carter, *Nature*, 1992, 358, 209.
20. S. K. Jana, A. K. Mandal, A. Kumar, H. Puschmann, M. Hossain and S. Dalai, *RSC Advances*, 2016, 6, 95888-95896.